Crystalline and Fiber Raman Lasers

T. T. Basiev[1], V. V. Osiko[1], A. M. Prokhorov[1], and E. M. Dianov[2]

[1] General Physics Institute Russian Academy of Sciences
Vavilova ul., 38, Moscow 119991, Russia
Tel/Fax: (7 095) 135-02-67
basiev@lst.gpi.ru

[2] Fiber Optics Research Center at the General Physics Institute, Russian Academy of Sciences
Vavilova ul., 38, Moscow 119991, Russia
Phone/Fax:(7 095) 135-05-66 dianov@fo.gpi.ru

Abstract. This chapter describes the state of the art of crystalline and fiber Raman lasers based on the simulated Raman scattering (SRS) effect in crystals and silica-based fibers. It includes historical and theoretical background, analysis of properties of known and newly developed high-efficient SRS crystals, such as $LiIO_3$, $Ba(NO_3)_2$, $NaNO_3$, $PbNO_3$, $CaCO_3$, KGW, $BaWO_4$, $SrWO_4$,$BaMoO_4$,$SrMoO_4$, $PbWO_4$, and germanosilicate and phosphosilicate fibers. A large set of data on IR Raman shifters and lasers operating in the CW, nanosecond, and picosecond regimes with low and high repetition rates is given. Some applications of Raman lasers in medicine, ecology, fiber optics, and communications are discussed.

1 Introduction (Historical and Theoretical Background)

Stimulated Raman scattering (SRS) was first observed 40 years ago by *Woodbury* and *Ng* [1] and was tightly related to the development of lasers, one of the most important discovery of the 20th century.

Previously, spontaneous Raman scattering (RS) was discovered simultaneously and independently by *Raman* and *Krishnan* in liquids [2] and by *Landsberg* and *Mandel'shtam* in crystals [3]. The stimulated processes of Raman scattering were accounted for in the general *Placzek* theory [4] developed soon after the discovery of the RS effect. However, only high-peak-power (megawatt) laser sources of light allowed one observe stimulated Raman scattering. SRS scattering was observed [1] when investigating Q-switching of a ruby laser with a nitrobenzene Kerr cell inside the laser cavity. In the laser spectrum, the authors observed an intense IR component with a frequency shifted from the laser line by $1345\,\mathrm{cm}^{-1}$, which was later explained by stimulated Raman scattering [5].

Since then, this interesting nonlinear phenomenon and its applications in laser spectroscopy and laser engineering have attracted great attention of physicists (see, for instance, the reviews [6,7,8,9,10,11,12,13,14,15,16,17,18] [19,20]). SRS can be used not only when studying the macroscopic behavior of

I. T. Sorokina, K. L. Vodopyanov (Eds.): Solid-State Mid-Infrared Laser Sources,
Topics Appl. Phys. **89**, 351–400 (2003)

materials under high-power laser radiation, which is important for developing high-power sources of coherent radiation at new wavelengths, but also in the microphysics of individual atoms, ions, and molecules.

It is convenient to present the RS process as a two-photon resonance, when the difference of the absorption (ν_{L}) and emission (ν_{S}) optical frequencies is equal to the frequency of an atomic or molecular vibration in Raman media:

$$\nu_{\mathrm{L}} - \nu_{\mathrm{S}} = \nu_{\mathrm{R}} \,.$$

Due to the two-photon nature, RS cross-sections are very small, $\sigma \approx 10^{-30}\,\mathrm{cm}^2$. That is why even today this effect is hard to observe in bulk materials without low-divergence high-power monochromatic laser pumping.

According to quantum theory [4,5,8,9,10], the intensity of stimulated Raman scattering is proportional to the occupation densities of the states of three interacting fields: laser pump photons (N_{L}), photons of the generated Stokes wave (N_{s}), and crystal phonons (molecular vibrations) in the ground (N_{g}) or excited (N_{e}) state ($N = N_{\mathrm{g}} - N_{\mathrm{e}}$)

$$\frac{dN_{\mathrm{S}}}{dz} \sim N_{\mathrm{L}} N_{\mathrm{S}} (N_{\mathrm{g}} - N_{\mathrm{e}}) \tag{1}$$

In the steady-state regime, when the pump duration t_{p} is much longer than the Raman mode dephasing time T_{R} ($t_{\mathrm{p}} \gg T_{\mathrm{R}}$), the intensity I_{S} of the SRS Stokes beam passing through the Raman medium with length l is given by

$$I_{\mathrm{S}}(l) = I_{\mathrm{S}}(0) \exp(g I_{\mathrm{L}} l) \tag{2}$$

where I_{L} is the intensity of the incident pump laser beam and g is the gain coefficient,

$$g = \frac{\lambda_{\mathrm{L}} \lambda_{\mathrm{S}}^2 N}{\pi c \hbar n_{\mathrm{S}}^2 \Delta\nu_{\mathrm{R}}} \left(\frac{\mathrm{d}\sigma}{\mathrm{d}\Omega} \right) . \tag{3}$$

Here λ_{L} and λ_{S} are the wavelengths of the pump laser beam and the Stokes Raman beam, respectively; c is the speed of light, n_{S} is the refractive index at the Stokes wavelength; $\Delta\nu_{\mathrm{R}}$ is the full width at half maximum of the Raman spectral line in s^{-1} units; and Ω is the solid scattering angle. The gain coefficient is the most important parameter for solid-state laser applications, and its magnitude is usually given in units of cm/GW. These expressions show that the intensity of the Raman beam increases with the intensity of the pump laser and with the interaction length. In addition, the gain is greatest for materials with a high density of scatters N, large Raman scattering integral cross-section $\mathrm{d}\sigma/\mathrm{d}\Omega$, and small Raman linewidth $\Delta\nu_{\mathrm{R}}$.

In the transient regime when the pump pulse duration is of the same order or shorter than the dephasing time T_{R} and the pump spectral width is broader than that of the Raman line ($t_{\mathrm{p}} < T_{\mathrm{R}}$; $\Delta\nu_{\mathrm{p}} > \Delta\nu_{\mathrm{R}}$), the analytical

expression for the Stokes intensity in the limit of large gain can be written as [12]

$$I_{\mathrm{S}}(l) = I_{\mathrm{S}}(0) \exp\left(-\frac{t_{\mathrm{p}}}{T_{\mathrm{R}}}\right) \exp\left\{2\left[I_{\mathrm{L}} t_{\mathrm{p}} l \frac{\lambda_{\mathrm{L}} \lambda_{\mathrm{S}}^2 N}{\hbar n_{\mathrm{S}}^2}\left(\frac{\mathrm{d}\sigma}{\mathrm{d}\Omega}\right)\right]^{\frac{1}{2}}\right\} . \tag{4}$$

Comparing expression (4) with (2) and (3) one can see that the transient Raman gain has a slower (square root) dependence on the crystal length and the total integral Raman scattering cross-section $\mathrm{d}\sigma/\mathrm{d}\Omega$ and does not depend on the Raman line broadening $\Delta\nu_{\mathrm{R}}$ at all. The linear gain dependence on the pump intensity for steady-state regimes changes to the square root dependence on the pump pulse energy ($E = I_{\mathrm{L}} t_{\mathrm{p}}$) for transient regimes.

Evaluations show that in the steady-state regime it is necessary to have a gain-pump-length product (increment) $gI_{\mathrm{L}}l = 25$ to reach the SRS threshold, when $I_{\mathrm{S}} \approx I_{\mathrm{L}}$. To meet this condition for gaseous and liquid SRS-active media, having $g = 1$–$3\,\mathrm{cm\,GW^{-1}}$ (for hydrogen $g = 1.5\,\mathrm{cm\,GW^{-1}}$, for nitrobenzene $g = 3\,\mathrm{cm\,GW^{-1}}$), one should use either a very long medium ($l = 30$–$100\,\mathrm{cm}$) or a pump intensity $I_{\mathrm{L}} > 1\,\mathrm{GW\,cm^{-2}}$.

The advantages of SRS-active molecular gases (H_2, N_2, O_2, CH_4) are optical homogeneity, simple formation of the active medium, high frequencies of SRS-active vibrations ($2\,000$–$4\,000\,\mathrm{cm^{-1}}$), and, as a result, large Raman frequency shift $\nu_{\mathrm{S}} = \nu_{\mathrm{L}} - \nu_{\mathrm{R}}$. Of great importance is the small homogeneous spectral width of an SRS gas vibration ($\Delta\nu_{\mathrm{R}} = 10^{-3}$–$10^{-1}\,\mathrm{cm^{-1}}$) and, hence, the relatively large peak RS cross-section for an individual molecule [12,13]. These advantages of molecular gases are balanced by several drawbacks. The first one is the low particle density even for pressures much higher than atmospheric ($N < 10^{21}\,\mathrm{cm^{-3}}$ for 10 bar), which must be compensated by a long interaction length (up to several meters). To ensure the high pump intensity (about $10^9\,\mathrm{W\,cm^{-2}}$) in such a long length is a quite difficult problem. The second limitation is the low thermal conductivity of gases, which makes one use bulky and expensive constant flow gas exchange systems. This considerably complicates the whole device, especially for high pressures.

The merits of liquid SRS media [12,13] are the simplicity of preparing an optical SRS cell and the high density of active particles ($10^{22}\,\mathrm{cm^{-3}}$). But the latter leads to the line broadening of vibrational transitions, particularly for high temperatures ($\Delta\nu_{\mathrm{R}} \approx 0.1\,\mathrm{cm^{-1}}$ for $T = 77\,\mathrm{K}$ and $\Delta\nu_{\mathrm{R}} \approx 1$–$4\,\mathrm{cm^{-1}}$ for $T = 300\,\mathrm{K}$), and reduces the RS peak cross-section, even for an individual molecule. However, these negative features do not eliminate the positive effect of high density, and, thus, molecular liquids have higher Raman gain ($g \approx 3\,\mathrm{cm\,GW^{-1}}$) and allow one to build much more compact devices in comparison with Raman gases.

The main drawbacks of liquid SRS-active media are the low thermal conductivity and a high value of $\mathrm{d}n/\mathrm{d}T$, resulting in significant thermal optical distortions accompanied by the problems of homogeneity of laminar flows. The high nonlinear refractive index n_2 causes self-focusing of the pump beam,

which reduces the interaction length, impairs the divergence, and may result in optical breakdown of the medium.

Cryogenic molecular liquids (N_2, O_2) possess high density, small line broadening, and large scattering cross-section and gain coefficient ($17\,\mathrm{cm\,GW^{-1}}$ [13]). When working with these liquids, the main problems are to keep the cryogenic temperatures of the SRS-active medium and provide thermal insulation of optical windows. In addition, most liquids exhibit high scattering losses due to suspended particles and bubbles, which distort the wave fronts of the pump and output SRS radiation.

Many of the above-mentioned problems can be overcome by using solid-state SRS media, in particular, single crystals and glass optical fibers. The high density of active particles in crystals ($N \approx 10^{23}\,\mathrm{cm^{-3}}$) defines the high SRS gain and, due to the short light–crystal interaction length, makes possible the development of the most compact laser systems [15,16,17,18,19,20,21,22]. The high symmetry of the atomic and molecular positions in crystals prevents variations in the frequencies and linewidths of Raman-active vibrations. Due to the small inhomogeneous broadening of the SRS-active line in the best crystals, the joined response of nuclear vibrations to the pump radiation is very strong, which manifests itself in a lower interaction threshold and in an increase of the SRS gain and conversion efficiency.

SRS crystals and Raman lasers are especially important for the mid and far IR regions, where the development of new active laser materials and solid-state lasers based on population inversion is limited by fast nonradiative multiphonon relaxation and low quantum yield.

The great number of natural and especially artificially synthesized crystals offers a great variety of properties, such as types of chemical bonds (ionic, ionic-molecular, covalent), transparency range (from 200 nm to 100 μm), vibrational frequencies active in the RS process (10–2000 $\mathrm{cm^{-1}}$), and integral cross-section of Raman scattering.

Search and development of new effective SRS crystals strongly depend on the insight into the intermolecular and molecule-to-phonon interaction, which defines the line broadening and the phase and population relaxation of vibrational excitations.

Let us summarize the advantages of SRS crystals and mention their shortcomings or limitations.

Advantages

- High concentrations of Raman scattering centers, $N = 10^{22}$–$10^{23}\,\mathrm{cm^{-3}}$
- High Raman gain, $g = 1$–$50\,\mathrm{cm/GW}$
- Small size, 1–5 $\mathrm{cm^3}$
- Great variety of Raman frequency shifts, from 10 to 2000 $\mathrm{cm^{-1}}$
- Wide optical transparency region, from 200 nm to 100 μm
- High thermal conductivity, $k = 1$–$20\,\mathrm{W/cm}$
- Low refractive index–temperature derivatives, $\mathrm{d}n/\mathrm{d}T = 10^{-6}$–$10^{-5}\,\mathrm{deg^{-1}}$
- Mechanical hardness

- Moisture resistance
- Broad range of temperature stability

Limitations

- Complicated individual technology for every single crystal synthesis, growth, orientation of crystal axes, optical treatment, and coating
- Limited pulsed laser damage threshold (0.2–1 GW/cm^2) and damage threshold due to average power
- High price of SRS crystals

Glass optical fibers are an excellent Raman medium. Although Raman gain in glass is typically three orders of magnitude lower than in crystals and liquids, low thresholds have been achieved by maintaining high power densities over long lengths of low-loss fibers.

2 Nanosecond SRS Based on $Ba(NO_3)_2$ Crystals

In the 1980s two new synthetic crystals were developed, which defined progress in SRS lasers for several years. These are barium nitrate $Ba(NO_3)_2$ crystal (see [18,19,20,23,24,25,26,27]) and potassium-gadolinium tungstate $KGd(WO_4)_2$ crystals (KGW) [21,22]. The former has a record-high gain (47 cm/GW) in the nanosecond steady-state regime and a high laser damage threshold of 10–20 J/cm^2 (see Table 1), but is very soft, plastic, and hygroscopic and has low thermal conductivity. The latter has much better mechanical characteristics and higher thermal conductivity and can be activated by rare earth laser ions, such as neodymium, erbium, etc. [22]. Unfortunately, this crystal has much lower laser damage threshold for nanosecond pulses and smaller steady-state RS peak cross-section. In spite of these drawbacks, KGW crystals found wide application in picosecond lasers, where the integral cross-section is much more important than the peak cross-section, and the laser damage threshold is much higher.

One of the first studies of visible SRS in synthetic nitrate crystals $Ba(NO_3)_2$, $Pb(NO_3)_2$, and $NaNO_3$ in comparison with natural $CaCO_3$ crystals was reported in [23]. The SRS crystals 15 mm long were studied in a single-pass scheme under 530-nm excitation. The pump laser, consisting of a Nd-glass master oscillator with passive Q-switching, a double-stage amplifier, and a second harmonic generator, produced pulses of green radiation with an energy of 0.8 J and duration of 15 ns. The pump energy density was increased from 1 J/cm^2 to the point of laser damage of the SRS crystal, which was 6–15 J/cm^2. For the $Ba(NO_3)_2$ crystal, the minimum SRS threshold energies were about 1 J/cm^2 for the first Stokes and 3 J/cm^2 for the second Stokes radiation, and the highest total conversion efficiency was equal to 26 %. The first Stokes maximum output energy was as high as 0.15 J at the pump energy density of about 8 J/cm^2, which was close to the surface

Table 1. Comparative SRS and thermo-mechanical characteristics of $Ba(NO_3)_2$, $KGd(WO_4)_2$, and $BaWO_4$ crystals

Characteristic	Raman crystal		
	$Ba(NO_3)_2$	$KGd(WO_4)_2$	$BaWO_4$
Raman frequency shift ν_R, cm^{-1}	1047	901; 767	924
Raman linewidth $\Delta\nu_R$, cm^{-1}	0.4	5.4; 6.4	1.6
Dephasing time T_R, ps	28	2.0	6.6
Gain coefficients, cm/GW:			
g(0.53 μm) steady-state (ns)	47	11	36–40
g(0.53 μm) transient (20 ps)	4.7	11	14.4
g(1.06 μm) steady-state (ns)	11	4	8.5
g(1.06 μm) transient (30–50 ps)	1.1	3	3.8
g(1.3 μm) steady-state (ns)			5.8
Transparency range, μm	0.33–1.8	0.3–5	0.255–5
Moisture resistance	Low	High	High
Thermal conductivity at 25 °C, W/K·m	1.17	2.5–3.4	3.0
Thermal expansion coefficient α/°C	13×10^{-6}	$(1.6–8.5) \times 10^{-6}$	6×10^{-6}
Hardness	19.2 ($NaNO_3$ Knoop)	4–4.5 (Moos)	4 (Moos) 400 (Knoop)

damage threshold. For the $Pb(NO_3)_2$ crystal, the SRS thresholds were approximately two times higher, while the maximum conversion efficiency was lower by about 20 %, and the first Stokes output of about 70 mJ was reached at the pump density of 6–7 J/cm^2, starting the bulk damage of the sample. The $NaNO_3$ and $CaCO_3$ crystals showed even higher SRS thresholds equal to about 4–5 J/cm^2, but also had higher laser damage threshold, of 14 J/cm^2. The output energies were measured to be 0.15 J with a conversion efficiency of 17 % for $NaNO_3$ and 0.12 J with 14 % efficiency for $CaCO_3$. Thus, by the first and second Stokes frequency shifts of 1045–1085 cm^{-1}, all these crystals can provide highly efficient yellow (560 nm) and orange (598 nm) visible radiation, with the best performance shown by the $Ba(NO_3)_2$ crystal.

Raman lasers based on $Ba(NO_3)_2$, $NaNO_3$, and $CaCO_3$ crystals under external pumping by nanosecond ($t_p = 10$ ns) 532-nm radiation were studied in [24,25]. In a flat–flat resonator 26 cm long with the reflectivity of mirrors $R_1 \approx 100$ % and $R_2 = 8$ %, the threshold pump densities were equal to 5–7 MW/cm^2 for nitrate crystals and 20 MW/cm^2 for calcites (the crystals were 5–8 cm long) [24]. These data well correlate with the directly measured SRS gain coefficients, $g_{Ba(NO_3)_2} = 47 \pm 5$ cm/GW, $g_{CaCO_3} = 13 \pm 3$ cm/GW.

At a pump density five times higher than the threshold one, the coefficient of the pump energy conversion to all the Stokes components reached

the maximum value of 50–65 %. Since the variations in R_2 from 4 to 20 % did not change the conversion efficiency, the exit face of the Raman crystal can be used instead of the output mirror. The maximum conversion coefficient in the $Ba(NO_3)_2$ crystal was 40 % for the first Stokes component and 25 % for the second Stokes for single-pass pumping. It was shown that the increase in the number of pump beam passes through the SRS crystal resulted in a better selection of the first Stokes radiation and an increase in the conversion efficiency to 50 % for the first Stokes component for two-pass pumping. The second Stokes component in a flat and unstable resonator can be efficiently suppressed by the application of the forward scattering geometry.

Transient stimulated Raman scattering in $Ba(NO_3)_2$ crystals was first studied in [28] under pumping by the Nd:YAG second harmonic. The pump pulse duration was about 22 ± 2 ps, which is less then the dephasing (transverse) relaxation time $T_R = 28$ ps of internal symmetrical vibrations of quasi-molecular $(NO_3)^-$ complexes of $Ba(NO_3)_2$ crystals. In the single-pass scheme, the SRS threshold intensities of $Ba(NO_3)_2$ crystals 50 and 40 mm long were estimated to be 1.1 and 1.45 GW/cm^2, respectively, which is much higher than for the steady-state nanosecond oscillation. This corresponds to an approximately 10-fold decrease of the picosecond Raman gain in comparison with steady nanosecond pumping. It should be noted that the overall conversion efficiency of a $Ba(NO_3)_2$ crystal at the pump density of 2 GW/cm^2 was 25 % for the first Stokes Raman shift (563 nm) and 5 % for the second Stokes (599 nm).

The above data, as well as a fast decrease in the SRS gain and fourfold increase in the SRS threshold with the pump wavelength changing from visible 532 to infrared 1064 nm, strongly restrict application of $Ba(NO_3)_2$ crystals for picosecond SRS in the infrared spectral region.

Solid-state Raman lasers, discretely or continuously tunable, are of special importance for the IR spectral region, where no dye lasers exist with high quantum yield and good photo and thermal stability, and only a few IR bands are covered by available tunable solid-state lasers based on activated crystals.

At the same time, SRS becomes more a complicated problem when moving to the IR spectral region, because the SRS gain coefficient can decrease fourfold with a twofold increase in the pump wavelength. For example, $Ba(NO_3)_2$ crystals have $g = 47\,\mathrm{cm\,GW^{-1}}$ for $\lambda = 532$ nm and $g = 11\,\mathrm{cm\,GW^{-1}}$ for $\lambda = 1064$ nm [26,27].

By the early 1980s, unique tunable lasers for the near IR range were developed employing LiF crystals with F_2^- and F_2^+ color centers [29,30,31,32]. These lasers were tunable in the IR region from 0.82 to 1.28 μm. To extend the tuning range further in the IR region, new SRS-active crystals, $Ba(NO_3)_2$ and $KGd(WO_4)_2$, were offered [33]. The investigations of [33] showed that $Ba(NO_3)_2$ crystals advantageously operate in the near IR range up to 1.7 μm with efficiencies as high as 60 % under nanosecond pumping with power densities well below the laser damage threshold. Further extension into the IR

is restricted by the $Ba(NO_3)_2$ fundamental absorption beginning at approximately 1.8 μm. The $KGd(WO_4)_2$ crystals have a much wider transparency region, up to 5 μm, and can also convert the IR radiation to the Stokes region, but the four times smaller steady-state gain coefficient and low radiation resistance restrain their application in nanosecond lasers.

The development of SRS shifters based on $Ba(NO_3)_2$ crystals enabled one to extent the spectral range of tunable solid-state lasers to the 1.3–1.7-μm IR region and, as a result, to develop a solid-state laser spectrometer for a very wide near-infrared region, from 0.82 to 1.66 μm. This spectrometer also covered the visible (0.42–0.82 μm) and UV (0.25–0.45 μm) regions by using frequency mixing and second and higher harmonics of IR radiation (Fig. 1) [32,33,34]. It was the first all-solid-state-laser spectrometer operating in all three spectral regions, UV, visible, and IR.

Interest in SRS lasers was rekindled in the early 1990s, when solid-state lasers based on impurity doped crystals found so wide application that this aroused the problem of how to prevent the human eye from being hurt by a laser beam. The laser wavelength safe for human eyes was standardized to be $\lambda = 1.54$ μm, and the radiation of the majority of lasers developed found themselves in the prohibited wavelength region with $\lambda < 1.5$ μm (as an example, Nd:YAG lasers operate at 0.53, 1.06, and 1.32 μm; ruby at 0.69 μm; alexandrite at around 0.78 μm; and Ti:sapphire at 0.7–1.1 μm). In this respect, the development of SRS frequency shifters for available laser radiation to the eye-safe wavelength of 1.54 μm is of great importance. Small atmospheric absorption and high transmittance of fibers at this wavelength allow wide applications of such devices for lidars, free space communication, and fiber links.

One of the simplest and most effective ways to get 1.54-μm radiation was proposed in 1993–1994 in [35,36,37,38,39,40,41,42], where a $Ba(NO_3)_2$ Ra-

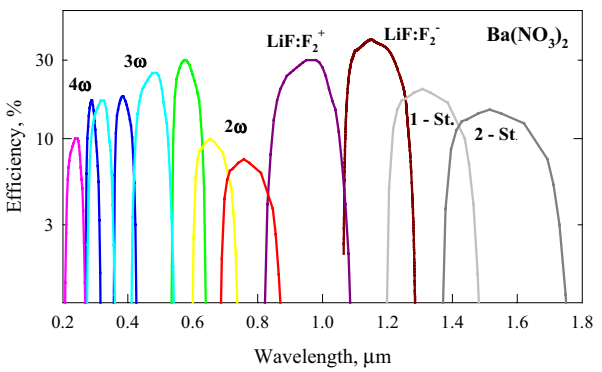

Fig. 1. Tuning curve of an all-solid-state laser based on LiF:F_2^+; F_2^- color center crystals, $Ba(NO_3)_2$ Raman shifters, and frequency doubling and mixing (for UV, visible, and near IR spectral regions)

man laser was pumped by the 1.064- and 1.320-μm radiation of a Q-switched neodymium laser. Under 1064-nm nanosecond pumping, a $Ba(NO_3)_2$ crystal 30–50 mm long in a compact cavity with dichroic mirrors, specially designed for optimum lasing of the first, second, and third Stokes waves, produced a single-mode radiation at new, including eye-safe, wavelengths (1.2–1.4 μm and 1.5–1.6 μm), with light-to-light conversion efficiency of 20–50 % (Fig. 2) [35,36,37,38].

The 1320-nm pumping provides a very good opportunity to build highly efficient, compact eye-safe Raman lasers ($\lambda = 1553$ μm), using only the first Stokes radiation conversion. A very high real conversion efficiency of 50 % was obtained in [38] (Fig. 3) at only a few millijoule (4–5 mJ) pulsed pumping of a 40 mm long $Ba(NO_3)_2$ crystal in a compact Raman laser cavity. In this case, a slope efficiency as high as 65 % and a quantum efficiency of 58 % were obtained in the TEM_{00} mode operation regime.

The 1.320 μm nanosecond intracavity pumping of a $Ba(NO_3)_2$ crystal, when the pump and Raman lasers had one common cavity or two optically coupled cavities, enabled increasing the conversion efficiency to the first Stokes at 1.5 μm up to 90 % [39,40,41,42]. In this case, the effect of nonlinear cavity dumping makes it possible to shorten the pump pulse a few times and increase the peak power. An important additional advantage of SRS lasers is that their output beam can have much better spatial quality and smaller beam divergence ("beam cleanup"), and, hence, higher brightness than the pump beam [36,37,38,43].

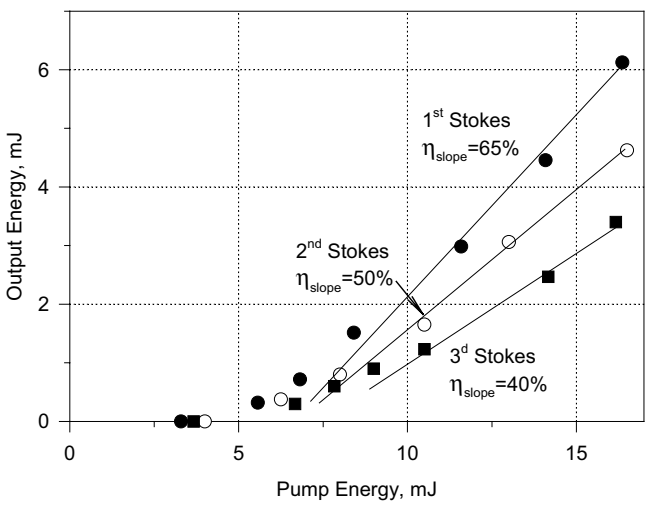

Fig. 2. The first (1197 nm), second (1369 nm), and third (1590 nm) Stokes output energy of $Ba(NO_3)_2$ Raman lasers with optimized coupling reflectivity (18, 26, and 25 %) for 1064-nm pumping and a 51 mm long SRS crystal

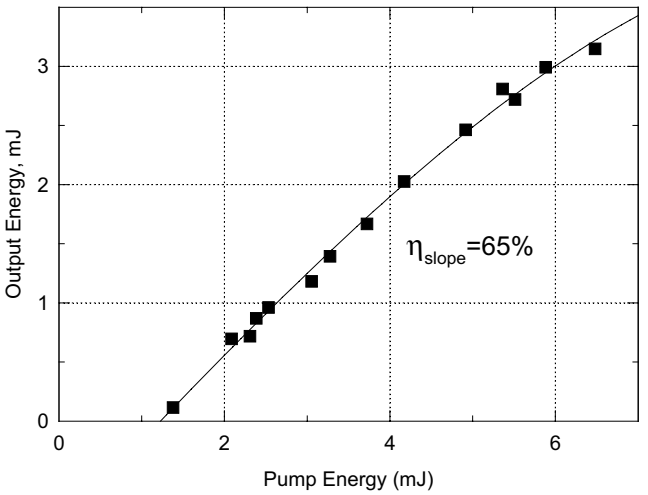

Fig. 3. Output energy of the first Stokes (1556 nm) radiation of an eye-safe Raman laser based on a 40 mm long $Ba(NO_3)_2$ crystal versus 1338-nm pump energy of a Nd:YAG laser

A diffraction-limited high-energy (0.25 J) eye-safe Raman laser with wavelengths of 1535 and 1560 nm was developed in 1995 [44,45] when an intracavity $Ba(NO_3)_2$ crystal was pumped by a high-power nanosecond Nd:YAG laser operating at 1.318–1.338 μm. The two standing-wave resonators, the pump laser cavity 69 cm long and the Raman cavity 20 cm long, were coupled by a dichroic beam splitter. Using a 50-mm uncoated $Ba(NO_3)_2$ crystal, the authors had 12 mJ of Raman laser output with 48 % conversion efficiency at the pump power of 25 mJ. The SRS pulse was about two times shorter than the 10-ns pump pulse. Nonlinear Raman beam cleanup was observed in the near and far fields of the 1.5-μm beam profile. The second Stokes radiation at 1.820–1.860 μm was generated through the cascaded SRS process. In an enhanced (more powerful) system with a Nd:YAG rod diameter of 7×110 mm and two flash lamp pump cavities, the output energy of diffraction-limited eye-safe radiation was increased to 0.25 J at the repetition rate of 1 Hz. The repetition rate was limited by the thermal effects due to low thermal conductivity of $Ba(NO_3)_2$ crystals.

In order to develop a marine-based lidar laser transmitter, operated around 580 nm, for very turbid water of a surf-zone, the authors of [46] have studied and optimized a $Ba(NO_3)_2$ Raman laser with intracavity pumping by a Nd:YLF laser and with second harmonic generation by a LBO crystal. With a Nd:YAG rod diameter of 7×76 mm and a T-shaped high-Q pump laser cavity coupled with a low-Q Raman cavity (400 and 85 mm in length, respectively), the authors realized nonlinear cavity-dumping regimes. They used a 20 mm long MgF_2 AR coated $Ba(NO_3)_2$ SRS crystal and the Raman

cavity output coupler with $R = 25\,\%$. At 50 J of the flash lamp pump energy and 10 Hz, the maximum output for the Raman wavelength of 1176 nm was 150 mJ, which was transferred into 90 mJ of yellow (588 nm) radiation by the LBO (type I) crystal 12 mm long. To stop pulse modulation and frequency cascading, the authors included a prism in the Raman cavity. In this case, they had 1.5-ns pulsed radiation at 588 nm wavelength, which is well suited for coastal water lidar applications.

3 $LiIO_3$ Raman Lasers

One of the first nonlinear crystals with good SRS properties that was used for developing Raman laser systems was lithium iodate, $LiIO_3$. This crystal is well known by its high nonlinear coefficient for frequency doubling, mixing, and parametric oscillation. In addition, its strong birefringence allows wide angular phase matching for various pumping wavelengths. This crystal also demonstrates a rather wide transparency spectral range (0.3–6.0 μm) and strong Raman scattering lines around 760 and 820 cm^{-1}.

A nanosecond $LiIO_3$ crystalline Raman laser operating in the IR region at a high repetition rate was first described in [47,48]. The pumping Nd:YAG laser operated in a quasi-CW mode at 1080 nm with repetition rate of 1–10 kHz and had a pulse duration of 100 ns. In a shared laser and Raman two-mirror cavity with a $LiIO_3$ SRS crystal 25 mm long, cut at $\theta \approx 20.5°$, the first Stokes radiation (the Raman shift $\nu_R = 818\,cm^{-1}$) had an average output power of 1.26 W and pulse duration of 50 ns. In a separate experiment, the second Stokes radiation at 1310 nm was obtained with a power of 0.55 W and pulse duration of 15 ns.

Using three-mirror coupled cavities, the authors of [48] had strong pulse shortening, $t_{p(1St)} = 4$–8 ns with an average output power of 0.9 W, peak power of 7 kW, and conversion efficiency of 77 %. After optimization, the second Stokes pulse duration was even shorter, $t_{p(2St)} = 2$ ns with average power of 0.2 W and peak power of 100 kW.

A picosecond Raman laser based on a $LiIO_3$ SRS crystal was studied in [49]. The authors used a Y-cut lithium iodate crystal 10 mm long and, as the source of synchronous pumping, a self-mode-locked neodymium phosphate glass laser operating at $\lambda = 1054$ nm. The pump pulses had a duration of 6–10 ps at the axial interval of 6.7 ns and the duration of the train envelop of about 200 ns.

The Raman laser cavity 1 m long was formed by an entrance edge mirror with $R_{1.05\mu} = 25\,\%$ and $R_{1.14c} = 98\,\%$, an output mirror with $R_{(1.05\mu,1.14\mu)} = 50\,\%$, and a two-lens intracavity telescope with the $LiIO_3$ crystal inside. The first Stokes component was observed at the wavelength of 1.143 μm with a frequency shift of 760 cm^{-1}. In the vicinity of the SRS threshold (1 mJ), the output train consisted of 25 pulses and had a total duration of 170 ns. Varying the Raman cavity length, the authors found that the maximum shortening

(by a factor of 7–8) of the SRS pulses in comparison with the pump pulses occurs when the Raman cavity length is equal to the length of the pump cavity. The minimum SRS pulse duration was 1 ps at the energy conversion efficiency of 30 %. The maximum conversion efficiency reached 40 %.

Recently, a series of studies [50,51,52,53,54] was devoted to practical development of Raman lasers based on a $LiIO_3$ crystal.

With flash-lamp quasi-CW (3 kHz) Nd:YAG intracavity pumping, the authors [50] got a 770 cm^{-1} Raman frequency shift and the first Stokes radiation at the wavelength of 1179 nm with average power of 1.8 W, pulse duration of 40 ns, and optical-to-optical conversion efficiency of 50 %.

By using a transversely diode-pumped Nd:YAG laser, the authors of [51,52,53] reached 2.7 W power of the first Stokes output radiation at 1155 nm with electrical-to-optical efficiency of 10 %.

The longitudinal diode pumping of the Nd:YAG-$LiIO_3$ Raman laser and optimization of thermal lensing resulted in an increase of the output average power of yellow radiation to 1.42 W at 20 ns pulse duration and 8-kHz repetition rate with electrical-to-optical efficiency of 7.5 % [54].

Unfortunately, till now no data have been published on the steady-state or transient SRS threshold and gain measurements in the $LiIO_3$ nonlinear crystal. Spontaneous Raman scattering characteristics can be found in [15,16,17,18] (see also Table 2 and the discussion below).

Among the limitations and shortcomings of $LiIO_3$ SRS crystals, we should mention low values of its thermal conductivity, moisture resistance, and laser damage threshold.

4 Picosecond Raman Lasers Based on KGW Crystals

A specific feature of picosecond Raman converters is that SRS has a nonstationary character when the pump pulse duration is of the same order or shorter than the time of phase relaxation of Raman vibrations. At the same time, the laser damage threshold of nonlinear crystals is much higher when the crystal is irradiated by picosecond laser pulses than by nanosecond ones, i.e. the picosecond operation mode allows pumping with a higher power density without crystal damage. As was shown earlier, for nonstationary pumping, the Raman gain coefficient sharply decreases in comparison with the steady-state regime, loses its dependence on the scattering peak cross-section and pump power, and keeps only the slow square root dependence on the integral Raman scattering cross-section and picosecond pump pulse energy density.

The first results on SRS in Nd:$KY(WO_4)_2$ (Nd:KYW) and Nd:$KGd(WO_4)_2$ (Nd:KGW) crystals were obtained in 1984 [55] under picosecond pumping. At the same time, it was also the first study where the Raman material worked simultaneously as an active and nonlinear SRS material.

Table 2. Parameters of spontaneous Raman scattering in crystals

Material	Lattice space group	Molecular group	Raman frequency ν_V (cm^{-1})	Raman linewidth Δ_ν (cm^{-1})	Integral cross-section (rel. u.)	Peak intensity (rel. u.)	Geometry of excitation scattering **K**	**E**
Diamond	O_h^7	-	1332.9	2.7	100	100	$//C_3$	$\perp C_3$
			Nitrates and Calcites					
$Ba(NO_3)_2$	T_h^6	$[NO_3]$	1048.6	0.4	21	63	$//C_4$	$//C_4$
$NaNO_3$	D_{3d}^6	-"-	1069.2	1.0	23	44	$//C_3$	$\perp C_3$
$CaCO_3$	D_{3d}^6	$[CO_3]$	1086.4	1.2	6.0	10.6	$//C_3$	$\perp C_3$
			Tungstates					
$CaWO_4$	C_{4h}^6	$[WO_4]$	910.7	6.95	52	18.6	$\perp C_4$	$//C_4$
$SrWO_4$	-"-	-"-	921.5	3	50	41	-	-
$BaWO_4$	-"-	-"-	926.5	1.63	52	64	-	-
$NaGd(WO_4)_2^*$	-"-	-"-	919	14*	-	-	-	-
$NaY(WO_4)_2^*$	-"-	-"-	918	15*	-	-	-	-
$Sc_2(WO_4)_3^*$	-	-"-	1024	15	-	-	-	-
$In_2(WO_4)_3^*$	-	-"-	1023	13	-	-	-	-
$LiIn(WO_4)_2^*$	-	-"-	920	8	-	-	-	-
$NaSr(WO_4)_2^*$			924	2.5				
$Na_2WO_4^*$	O_h^7		929.2	1.8				
$KGd(WO_4)_2$	C_{2h}^6	$[WO_6]$	901	5.4	50	35	$\perp C_2$	$\perp C_2$
-"-	-"-	-"-	901	5.4	43	30	$\perp C_2$	$//C_2$
-"-	-"-	-"-	768	6.4	19	9.2	$\perp C_2$	$\perp C_2$
-"-	-"-	-"-	768	6.4	59	37	$\perp C_2$	$//C_2$
$KY(WO_4)_2$	-"-	-"-	905.6	7	46	35	$\perp C_2$	$\perp C_2$
-"-	-"-	-"-	905.6	7	41	30	$\perp C_2$	$//C_2$
-"-	-"-	-"-	767.4	8.4	17	10	$\perp C_2$	$\perp C_2$
-"-	-"-	-"-	767.4	8.4	58	35	$\perp C_2$	$//C_2$
$KYb(WO_4)_2$	-"-	-"-	908	7.4	48	34	$\perp C_2$	$\perp C_2$
-"-	-"-	-"-	908	7.4	48	34	$\perp C_2$	$//C_2$
-"-	-"-	-"-	757	15**	18**	13.8**	$\perp C_2$	$\perp C_2$
-"-	-"-	-"-	757	15**	58**	30**	$\perp C_2$	$//C_2$
			Molibdates					
$CaMoO_4$	C_{4h}^6	$[MoO_4]$	879.3	5.0	64	34	$\perp C_4$	$//C_4$
$SrMoO_4$	-"-	-"-	887.7	2.8	55	51	$\perp C_4$	$//C_4$
$BaMoO_4$	-"-	-"-	892.4	2.1	52	64	$\perp C_4$	$//C_4$
			Iodate and Niobates					
$LiIO_3$	C_6^6	$[IO_3]$	821.6	5.0	54	25	$//C_2$	$\perp C_2$
$LiNbO_3$	C_{3v}^6	$[NbO_6]$	872	21.4	44	5	$//C_3$	$\perp C_3$
-"-	-"-	-"-	632	27	166	18	$\perp C_3$	$//C_3$
-"-	-"-	-"-	250	28	-	22	$\perp C_3$	$//C_3$
$LaNbO_4$	C_{2h}^3	$[NbO_4]$	805	9	22	7.1	$\perp C_2$	$//C_2$
			Phosphates					
$Ca_5(PO_4)_3F$	C_{6h}^2	$[PO_4]$	964.7	2.8	3.4	3.8	$\perp C_6$	$//C_6$
$Sr_5(PO_4)_3F$	-"-	-"-	950.3	2.8	3.4	3.8	$\perp C_6$	$//C_6$
$LiPO_4^*$	-	-"-	951	7.7	-	-	-	-
			Other					
$NaClO_3^{***}$	-	$[ClO_3]$	937	4.9**	-	-	-	-
$NaBrO_3^{***}$	-	$[BrO_3]$	799.5	2.5**	-	-	-	-
NH_4Cl^{***}	O_h^1	$[NH_4]$	1712	6	-	-	-	-
-"-	-"-	-"-	3052	85**	-	-	-	-
$NH_4SO_4^{***}$	-	$[SO_4]$	976.5	3.5	-	-	-	-
$Ba_3(B_3O_6)_2$	C_{3v}^6	$[B_3O_6]$	636	4.5	1	0.6	$//C_3$	$\perp C_3$
SiO_2	D_3^6	$[SiO_4]$	464	7	2.2	1.2	$\perp C_3$	$//C_3$

* policrystalline sample
** line with inhomogeneous splitting
*** crystal without orientation

At about 20-J flash lamp pump energy, active elements 5 mm in diameter and 50 mm long oscillated at the fundamental Nd^{3+} wavelength of 1067 nm in a single-mode regime, producing a train of about 10 ultrashort pulses, each having a pulse width of 11–12 ps at the spectral width of 1.8 cm^{-1} and energy of 0.5 mJ. The efficiency of stimulated Raman self-conversion to the first Stokes component ($\lambda = 1182.7$ nm) for a single picosecond pulse from the beginning of the train was 6.14 % of the total energy and reached 35 % in the middle of the train. In the case when two Nd:KYW crystals were used (one as the lasing and self-converting Raman master oscillator, and the second as the synchronously laser-pumped Raman amplifier (without flash lamp pumping), the authors had a maximum conversion efficiency $\eta_{1St} = 37$ % to the first Stokes, $\eta_{2St} = 16$ % to the second Stokes ($\lambda_{2St} = 1323.7$ nm), and $\eta_{aS} < 5$ % to the anti-Stokes ($\lambda_{aS} = 947.9$ nm). When the Nd:KYW amplifier was additionally pumped by 30 J of flash lamp radiation, the total output energy increased to 11 mJ.

For two Nd:KGW crystals 50 mm long used in one laser cavity, the conversion efficiency of the whole train to the Raman scattering radiation was not so high, $\eta_{1St} = 3.84$ % ($\lambda_{1St} = 1180.5$ nm), probably due to low quality of the crystals, and was improved with a SRS amplifier to $\eta_{1St} = 16.58$ %, $\eta_{2St} = 0.96$ %, and $\eta_{aS} = 0.03$ %.

The authors also briefly mentioned an oscillation observed in Nd:$KLa(MoO_4)_2$ and Nd:$NaLa(MoO_4)_2$ crystals. The pulse duration at the fundamental wavelength was 5–6 ps and at the first Stokes component, 1.5–2.5 ps, with the conversion efficiency $\eta_{1St} = 40$ %.

Almost simultaneously with [55], the intracavity Raman oscillation on Nd:KGW crystals was reported in [56]. The authors studied the frequency doubling of the picosecond radiation of a Nd:KGW laser with passive mode locking. New radiation wavelengths, of 1180 and 1320 nm, were found corresponding respectively to the first and second Stokes components of the SRS conversion of the Nd^{3+} fundamental wavelength (1067 nm) in a Nd:KGW crystal with a frequency shift of 900 ± 10 cm^{-1}. This was proved by the SRS radiation of the Nd:KGW crystal that was placed in the picosecond Nd:YAG laser cavity and was not flash lamp pumped. Estimation of the SRS conversion efficiency showed that only 10 % of the total energy belongs to the 1180-nm radiation and the rest (90 %) belongs to the 1067-nm radiation. Therewith, the SRS pulse duration was 3.8 ± 0.4 ps, which was considerably shorter than the pump pulse, by a factor of 2.5.

The SRS of undoped KGW crystals with different orientation in an external pumping scheme under 30-ps Nd:YAG laser pumping was studied later in [57]. In the spectral region from 1.06 to 1.32 μm, the SRS radiation of 12 new spectral lines with different combinations of Stokes shifts of 84, 767, and 901.5 cm^{-1} was recorded. The normalized thresholds and gain coefficients for different polarization orientations were measured. The maximum gain coefficients were measured to be 6.4 cm/GW for the 901.5 cm^{-1} Stokes frequency

shift and 4.3 cm/GW for 767 cm^{-1}. With increasing pump density, the SRS radiation of higher Stokes components, up to the fourth component with wavelength $\lambda_{4St} = 1730$ nm, was recorded.

The SRS pulse compression in Nd:KGW and Nd:KYW picosecond lasers was specially investigated in [58,59]. In a cavity 1.3 m long formed by a back dichroic mirror with $R_{1064\,nm} = 99.94\,\%$ and $R_{1180\,nm} = 72.6\,\%$ and by a glass plate as the output coupler, the first Stokes radiation comprised 22–40 % of pump pulse energy at the middle of the pulse train, the first Stokes pulse duration was as short as $t_{1St} = 1.3$ ps, and the pump pulse duration was also shortened to 3.9 ps. Application of the SRS amplifier on a Nd:KGW crystal with synchronous laser pumping in a passive regime (without flashlamp pumping of Nd^{3+} ions) allowed the authors to shorten the Stokes pulse to the minimum value of 0.9 ps and increase the conversion efficiency above 40 %. For active amplifying, the Stokes pulse duration grew continuously from 1.1 to 6 ps as the energy E_p of Nd:KGW amplifier pumping increased from 25 to 80 J. The duration of the Nd laser fundamental radiation pulse decreased from 10 to 4.4 ps.

A detailed review of the KGW crystal structure, lattice cell parameters, atomic positions and coordinates and interatomic distances can be found in [60,61]. Spectroscopic study of spontaneous and stimulated Raman scattering in KGW crystals with different orientation of the pump beam direction and polarization with respect to the crystallographic axes was also presented. The Stokes components of stimulated Raman scattering, from the first (1162.2 nm) to the fourth (1734.8 nm) ones, were observed under pumping by the 1064-nm radiation of a Nd:YAG laser with pulse duration of 30 ps. The threshold power was 4.8–24.3 GW/cm^2. The threshold pump density for the KGW first Stokes with shifts of 767 and 901.5 cm^{-1} was measured for different orientations and compared with those measured for $CaWO_4$ and $Ba(NO_3)_2$ crystals [60]. The normalized SRS threshold for KGW was measured to be from 3.9 to 14.8 GW/cm^2 depending on the crystal orientation, which was much less than 23–25 GW/cm^2 for $CaWO_4$ crystals. The SRS threshold pump density measured for the $Ba(NO_3)_2$ crystal to be 6.2 GW/cm^2, is much less than that for $CaWO_4$, but higher than the minimum value for KGW at optimum orientation.

The nonstationary gain coefficient calculated from the measured thresholds turned out to be minimal for $CaWO_4$ crystals ($g = 1$–1.1 cm/GW), four times higher for $Ba(NO_3)_2$ crystals ($g = 4$ cm/GW), and highest for KGW crystals for optimum orientation $p[mm]p$ ($g = 6.4$ cm/GW for the 901.5 cm^{-1} Stokes shift). For the KGW Stokes shift of 767 cm^{-1} and the orientation $q[pp]q$, this value was $g = 5.2\,cm^{-1}$. The above data on KGW and KYW Raman lasing properties demonstrate very efficient operation of these crystals in the pico- and subpicosecond regimes of oscillation, where the high density pumping (1–10 GW/cm^2) can be used without radiation damage of the crystal. These crystals demonstrate the multiwavelength frequency shift of

coherent radiation in the most hard-to-reach IR region from 1 to 1.7 μm with a high conversion efficiency (about 40 %) and very effective radiation pulse shortening (more than 10 times) down to subpicosecond pulse durations.

5 Nanosecond Raman Lasers Based on KGW Crystals

The main problem that arises when one tries to use KGW crystals as Raman shifters for nanosecond IR laser radiation is a rather high SRS threshold (due to the low Raman gain) in combination with the low laser damage threshold at nanosecond pumping. The narrow gap between the SRS and laser damage thresholds essentially restricts the SRS conversion efficiency and imposes strong requirements upon the pump radiation profile and the optical quality of the crystal and all the elements of the Raman cavity.

The first paper where the authors succeeded in realizing nanosecond intracavity SRS generation on a Nd:KGW crystal was [62]. The pulse duration of the fundamental radiation was $t_p = 7.5$ ns, and the duration of the first Stokes pulse at 1180 nm was measured to be threefold shorter, $t_{SRS} = 2.5$ ns. The intracavity SRS threshold was estimated to be 150–300 MW/cm^2. However, no data on the conversion efficiency and output energy were reported.

Nanosecond SRS in a KGW crystal in a single-pass scheme with an external pumping was also studied in [63]. The steady-state SRS gain coefficients for both Stokes shifts, of 901.5 cm^{-1} and 767.3 cm^{-1}, were found to be 6 cm/GW when pumped by a Nd:YAG laser with the radiation wavelength of 1064 nm. For nanosecond ($t_p = 10$ ns) pumping by a Nd:KGW laser in a single-pass scheme, the total efficiency of SRS conversion to both (first and second) Stokes was 70 % with the output energy of 10 mJ and did not depend on whether the Stokes shift frequency was 767.3 or 901.5 cm^{-1}.

Application of KGW crystals for SRS frequency shifting of nanosecond radiation with longer wavelength, 1.1–1.4 μm, where the gain coefficient is much weaker, was first demonstrated in [33]. A KGW crystal 40 mm long was used for nanosecond SRS frequency conversion of a tunable solid-state LiF:F_2^- color center laser MALSAN-201. The LiF:F_2^- color center laser radiation was tuned from 1.1 to 1.23 μm and provided the pump density of about 1 GW/cm^2 inside the SRS crystal. Using the single-pass Raman shifting scheme with the pump pulse duration of 8 ns, energy of about 20 mJ, and spectral width of 0.1 cm^{-1}, the authors observed tunable radiation in new spectral regions, 1.23–1.37 μm (first Stokes) and 1.43–1.6 μm (second Stokes). The maximum conversion efficiency reached 30 % for the first Stokes and 20 % for the second. These results were among the first experiments on solid-state Raman lasers operated in the eye-safe spectral region (≈ 1.54 μm). It should be noted that the laser damage threshold was only 2–3 times higher than the SRS threshold, which strongly limited the reported application of KGW crystals.

Ten years later, a compact flash lamp pumped solid-state laser for a range finder operating in the eye-safe spectral region at 1538 nm was developed

in [64,65] with application of SRS in a Nd:KGW active crystal self-pumped by 1350-nm (fundamental wavelength) Nd^{3+} laser radiation. The authors used Nd:KGW active-nonlinear elements with dimensions of $\varnothing 3 \times 50$ and $\varnothing 4 \times 65$ mm. The cavity mirrors had reflectivity $R_1 = R_2 = 99.99\,\%$ at the fundamental wavelength of 1350 nm, and the output mirror had 35–40 % reflectivity at the first Stokes wavelength of 1538 nm. Passive polymer and electrooptical $LiNbO_3$ Q-switches were used.

In the case of the Nd:KGW crystal with small dimensions, 3 mm in diameter and a length of 50 mm, the threshold pump energy of single-pulse operation changed from 2.5 to 5.5 J, and the energy of the 40-ns SRS pulse increased from 1 to 6 mJ, as the passive Q-switch transmission changed from 45 to 33 %. The KGW crystal with dimensions of 4 mm in diameter and a length of 65 mm allowed increase of the output energy to 9 mJ at the pump energy of 7.5 J. With electrooptical Q-switching by a Brewster cut $LiNbO_3$ crystal, the output energy of 12-ns pulses reached 13.5–15 mJ at the pump energy of 10 J. The overall efficiency was quite high, 0.15 %.

Using diode laser pumping of Nd-doped laser crystals, one can build compact and efficient solid-state lasers for the IR and green spectral regions. A transversely diode pumped $Nd:KGd(WO_4)_2$ Raman laser with self-frequency conversion was described in [66]. An AlGaAs/GaAs quasi-CW diode laser operating at 808 nm with a power of 300 W and pulse duration of 300 μs was used for side pumping of a $Nd:KGd(WO_4)_2$ crystal rod 4 mm in diameter and 22 mm in length. The plane-concave Raman laser cavity with an acousto-optical Q-switch inside had a high reflectivity for the fundamental wavelength (1067 nm) and the output coupler transmission of 5 % for the first Stokes wavelength (1162 nm). As a result, the first Stokes pulsed radiation had an energy of 0.1 mJ at a pulse duration of 50 ns, while the pump pulse duration was 140 ns at the repetition rate of 47 Hz. The second harmonic radiation (581 nm) was generated with a 30 % efficiency by a LiB_3O_5 crystal with non-critical phase matching at a temperature of 54 °C.

Recently, the intracavity self-frequency conversion in microchip Yb:KGW and Yb:KYW crystals was reported by two groups of authors [67,68]. They used 1.7 and 1.1-mm thick plates of Yb-doped laser crystals, pumped by a 980-nm laser diode, and a Cr^{4+}:YAG plate as the saturable absorber. For output coupler reflectivity of 7 and 5 %, the authors obtained nanosecond pulses of the first Stokes radiation at 1139-nm wavelength with an average power of 7 and 2 mW and repetition rate of 17 and 49 kHz, respectively.

The above historical review of the best SRS materials for nano- and picosecond Raman lasers shows that till the mid 1990s, there was no clear understanding of why one SRS material is better for nanosecond operation and another material operates better in the picosecond regime. There was no complete comparative analysis of the main fundamental properties of SRS materials, which would allow one to select the most suitable materials among

the known synthetic crystals or to develop SRS materials with required properties.

6 Search for New SRS Materials and Comparative Spectroscopy Study

New SRS converters and lasers could not be purposefully developed without a deep insight into the physics of Raman-active vibrational excitations, which determine the nature of light scattering and its properties. In the early 1980s, the complex inhomogeneous nature of RS resonance in fused quartz at a frequency of $460\,\mathrm{cm}^{-1}$ was revealed in [69]. Using LiF:F_2^- color center tunable lasers and the techniques of biharmonic pumping ($\lambda_1 = 1.064\,\mu\mathrm{m}$ and $\lambda_2 = 1.119\,\mu\mathrm{m}$), the authors eliminated the inhomogeneous broadening and, using RS amplification spectroscopy, for the first time measured the homogeneous width ($16\,\mathrm{cm}^{-1}$) of the inhomogeneously broadened ($\approx 200\,\mathrm{cm}^{-1}$) vibrational spectrum of fused quartz. At the same time, a very efficient pump-to-Stokes radiation conversion (38 %) was observed in 2–3-m long silica fibers.

The physics of SRS processes in the unique $Ba(NO_3)_2$ crystal at various temperatures, down to liquid-helium, was studied in [70] by the methods of nanosecond SRS amplification spectroscopy with high spectral resolution and in [71] by transient picosecond spectroscopy of Coherent Anti-Stokes Raman Scattering (CARS). The unique properties of $Ba(NO_3)_2$ crystal, namely, extremely low SRS threshold and high gain and efficiency, were not understood before. It was found that the high-frequency ($1047\,\mathrm{cm}^{-1}$) totally symmetric Raman active vibration A_{1g} of NO_3 quasi-molecular groups exhibits anomalously low homogeneous and inhomogeneous line broadening ($\Delta\nu = 0.4\,\mathrm{cm}^{-1}$ at room temperature), which reflects the anomalously weak coupling with other quasi-molecular and lattice vibrations [70]. The directly measured dephasing time T_R of the A_{1g} vibration proved to be surprisingly long ($T_{\mathrm{R}(300\,\mathrm{K})} = 28\,\mathrm{ps}$) at room temperature and almost ten times longer at liquid helium temperatures ($T_{\mathrm{R}(11\,\mathrm{K})} = 220\,\mathrm{ps}$) [71]. These values are several tens of times higher than those for diamond, calcite, $NaNO_3$, and other SRS crystals.

As the temperature increases to 400–600 K, the homogeneous line broadening $\Delta\nu_\mathrm{R}(T)$ and dephasing rate T_R^{-1} of $Ba(NO_3)_2$ rapidly grow, but still keep much lower values than for other matrices. Experimental data on the dephasing rate T_R^{-1} versus temperature, obtained by RS amplification and picosecond CARS at $T = 11$–$600\,\mathrm{K}$, were described by the theory of multiphonon decay, absorption, and dephasing of vibrational excitations and lattice phonons in a crystal. The analysis showed that the anomalously long lifetime of the A_{1g} vibration in $Ba(NO_3)_2$ crystals mainly resulted from the absence of three-phonon decay processes (when one high-frequency RS-active vibration decays into two vibrations with lower frequencies) [70,71]. At temperatures from 11 to 300 K, these three-phonon relaxation and dephasing

processes dominate over all the others in most SRS active materials (except A_{1g} Raman vibrations in $Ba(NO_3)_2$) and cause high dephasing rates and significant homogeneous line broadening [20]. It was found that the dephasing and broadening in $Ba(NO_3)_2$ crystals occurs not only due to the allowed four-phonon decay processes $\nu_{1047} \rightarrow \nu_{817} + \omega_{144} + \omega_{81}$ dominating at low temperatures (4–77 K) but is also due to the six-phonon decay processes $\nu_{1047} \rightarrow \nu_{731} + 4\omega_{81}$. The latter, despite a substantially lower probability, exhibit a rapid growth with increasing temperature and make a significant contribution to the line broadening at above-room temperatures [70,71]. Nevertheless, the sum of these two high-order processes demonstrates much less broadening and rate of dephasing than the low-ordered three-phonon processes in other SRS materials.

Due to the extending application of SRS crystals, the great variety of their properties, and the wide scatter in published data, in recent years a demand arose for comparative quantitative analysis of SRS-active crystals, which is very important for the search and development of new efficient SRS crystals. Such a detailed analysis both of known SRS crystals and new crystals with promising properties for SRS lasers was performed in [72,73,74,75,76]. Carbonate, nitrate, phosphate, tungstate, niobate, iodate, bromide, borate, and silicate crystals were analyzed. The frequencies and linewidths of the most intense and narrow quasi-molecular Raman vibrations of $[CO_3]$, $[NO_3]$, $[WO_4]$, $[MoO_4]$, $[NbO_6]$, $[NbO_4]$, $[IO_3]$, $[PO_4]$, $[ClO_3]$, $[B_3O_6]$, $[BrO_3]$, $[SiO_2]$, $[SO_4]$, and $[NH_4]$ anion groups were compared.

The relative intensities (integral and peak) of spontaneous RS lines were measured for more than 30 synthetic crystals in comparison with the reference diamond crystal (100 %). The RS line intensities were studied for various orientations of the crystals with respect to the exciting and scattered beams (see Table 2) [72,73,74,75,76].

It was shown that among the above-listed crystals only the iodate, niobate, tungstate, and molybdate crystals possess significant integral scattering cross-sections (40–60 %) for high-frequency RS lines (600–900 cm^{-1}). With the exception of lithium niobate crystals (166 %), these values are somewhat lower than for diamond (100 %) but several times larger than for the known SRS-active crystals of calcite (6 %) and nitrates (20 %). As one can see from (3) and (4), the integral RS cross-section is directly responsible for the SRS threshold and gain both in the steady-state and transient regimes and at the same time demonstrates slow variation for crystals with the same anion group.

A different situation was observed for the peak cross-sections of Raman scattering, which determine the SRS threshold and gain coefficient in the steady-state regime under nano- and subnanosecond pumping $t_p > 10\,T_R$. For example, the uniquely small broadening of RS lines in nitrate crystals results in record high peak values (44–63 %), though they have quite moderate integral RS cross-sections (21–23 %).

The analysis of the data given in Table 2 shows that the best crystals for low-threshold SRS frequency converters should have both a large integral RS cross-section and small RS transition broadening. Two promising classes for this purpose are tungstates and molybdates, which possess large integral RS cross-sections (40–60 %) and a great variety of line broadenings (from 1.6 to 15 cm^{-1}).

Since the line broadening (both due to upconversion and decay dephasing) of high-frequency SRS-active vibrational modes relates to their interaction with lattice phonons, the authors of [73,74] selected the crystals with the heaviest cations to reduce the frequencies of lattice phonon modes. In [73,74,77] simple tungstates of alkaline-earth metals (Ca, Sr, and Ba) with a scheelite structure were synthesized and investigated in detail. As can be seen from Table 2, the $CaWO_4$ SRS crystal frequently encountered in the scientific literature [7,60] has a moderate peak scattering cross-section, equal to 18 %, which is 3.5 times smaller than in the $Ba(NO_3)_2$ crystal and almost two times smaller than in $KGd(WO_4)_2$. This results from the significant broadening of its RS line, $\Delta\nu = 6.95\,cm^{-1}$ at room temperature. Replacement of light calcium cations for heavier strontium and barium cations resulted in a much lower relaxation rate and several times narrower spectral line (1.63 cm^{-1}) of $BaWO_4$ Raman vibrations at room temperature.

As the cation mass increases in the sequence Ca, Sr, and Ba, the maximum frequency ω_{lat} of lattice phonons in fact decreases, from 274 to 194 cm^{-1}. In addition, the increase of the lattice constant and cation radius results in the higher frequency of the totally symmetric A_{1g} Raman mode of the $[WO_4]^{2-}$ quasi-molecular complex (see Table 2). These two factors weaken the vibronic–lattice interactions and considerably narrow the spectrum of Raman vibration, which should manifest itself in a growth of the peak scattering cross-section and steady-state SRS gain.

The detailed study of RS fine structure of the A_{1g} oscillation mode in scheelites [78] shows that due to the largest values of lattice constants and W–W distances for the $BaWO_4$ crystal (as well as for $Ba(NO_3)_2$), the Davydov splitting (DS) for these crystals is very small, $\Delta E_{DS} \approx 0.5$–$1\,cm^{-1}$. The very low acoustic phonon density of states at this frequency, $h\omega_{ph} = \Delta E_{Ds} = 0.5$–$1\,cm^{-1}$, cannot provide fast dephasing processes and strong broadening of these Davydov-split components by means of direct single phonon bridge processes. Conversely, in $CaWO_4$, $PbWO_4$, and partly in $SrWO_4$ crystals with smaller lattice constants, the Davydov splitting was found to be much higher: 50, 32, and 28 cm^{-1}, respectively. This can explain the much faster dephasing and stronger broadening (6.9, 4.7, and 3 cm^{-1}) in these crystals due to direct single-phonon bridge processes from one DS component to another with absorption or emission of acoustic phonons of frequencies 28–50 cm^{-1}, whose density of states can be rather high ($\rho \approx \omega_{ph}^2$).

Similar regularities were observed in the series of alkaline-earth molybdates with a scheelite structure, $CaMoO_4$, $PbMoO_4$, $SrMoO_4$, and $BaMoO_4$.

Table 2 demonstrates the relative values of integral and peak scattering coefficients. As is seen, even with the broader RS lines, the new crystals $BaWO_4$ and $BaMoO_4$ can surpass the unique $Ba(NO_3)_2$ crystal in the peak cross-section, while the $SrWO_4$ and $SrMoO_4$ crystals are only slightly below.

The data on the peak cross-sections of spontaneous RS found by the comparative study were subsequently confirmed by direct measurements of SRS gain and SRS threshold [75,76,77,78,79,80]. This gave high potentiality of the newly developed crystals for application in SRS amplifiers and lasers, which will be discussed below.

7 New $BaWO_4$ SRS Crystals

The newly developed $BaWO_4$ crystals for stimulated Raman scattering exhibit many advantages in comparison with the two previously discussed best synthetic crystals, $Ba(NO_3)_2$ and $KGd(WO_4)_2$ (the characteristics of these crystals are compared in Table 1).

As one can see, the $BaWO_4$ crystal has much higher hardness, thermal conductivity, and moisture resistance than $Ba(NO_3)_2$. The transparency range in IR is also much wider, up to 5 μm, for $BaWO_4$ than for $Ba(NO_3)_2$ crystals, which is promising for mid-IR Raman laser development. The Raman scattering integral cross-section of $BaWO_4$ is at least two times higher, which is important for picosecond application, where $BaWO_4$ can provide much higher gain than $Ba(NO_3)_2$. The extremely small Raman line broadening ($0.4\,cm^{-1}$) in $Ba(NO_3)_2$ results in the record-high gain in the nanosecond (steady-state) regime of SRS, but at the same time restricts the steady-state regime on the picosecond time scale. As a result, the Raman gain of $Ba(NO_3)_2$ falls down steeply with shortening the picosecond pulse duration due to the transient character of SRS.

The $BaWO_4$ crystal exhibits only a slightly smaller SRS peak cross-section and gain coefficients as compared to those of $Ba(NO_3)_2$ for nanosecond pulses, but, due to the four times larger linewidth ($1.6\,cm^{-1}$) and correspondingly four times shorter dephasing time T_R, its steady-state regime can be extended to four times shorter laser pulses on the picosecond time scale.

Comparing the $BaWO_4$ crystal with $KGd(WO_4)_2$, one can see almost equally good hardness, thermal conductivity, moister resistance, and transparency range. The integral cross-sections of these two crystals are also quite similar and high. A difference can be found only in the line broadening and the dephasing time. Due to the three times broader Raman line, the $KGd(WO_4)_2$ crystals have much lower nanosecond (steady-state) SRS cross-section and gain coefficient than $Ba(NO_3)_2$ and $BaWO_4$ crystals. Even for the picosecond region 10^{-11}–10^{-9} s, the new $BaWO_4$ crystal can show much better SRS operation than $KGd(WO_4)_2$. Only at few-picosecond or subpicosecond pumping, can KGW crystals overtake the $BaWO_4$ crystal in gain

and efficiency due to the deeper transient behavior and faster gain decrease of $BaWO_4$ in comparison with KGW.

Similar properties are demonstrated by the $SrWO_4$ and $SrMoO_4$ crystals, whose line broadening and dephasing times lie between those of $BaWO_4$ and KGW crystals and define the intermediate values of the $SrWO_4$ and $SrMoO_4$ SRS cross-section and Raman gain, which are better than for KGW and poorer than for $BaWO_4$ in the nano- and picosecond steady-state regime.

8 $BaWO_4$ and $SrWO_4$ Nanosecond Raman Lasers

The IR SRS laser oscillation using newly developed $BaWO_4$ crystals and two well-known nonlinear crystals, was comparatively studied in [79], using a 9 cm long Fabry–Pérot cavity formed by two plane dielectric mirrors, an input mirror with $R_{1.064} < 5\,\%$ and $R_{1.1–1.25} > 98\,\%$ and an output mirror with $R_{1.0–1.2} \approx 55\,\%$.

A pulsed transverse single-mode Nd:YAG laser passively Q-switched by a $LiF:F_2^-$ crystal was used as the pump source. The pump laser produced 12-ns pulses at 10 Hz repetition rate. The pump beam was focused on the center of the SRS crystal by a lens with a focal length of 50 cm. The beam focal diameter was measured with a CCD camera to be 90 μm at half maximum. The beam shape was close to Gaussian.

The Raman laser energy efficiency reaches 26 % for $Ba(NO_3)_2$ and 20.5 for $BaWO_4$. In both cases, the slope efficiency exceeds 75 %, and the laser thresholds are very close. At the same time, no efficiency saturation is observed for $BaWO_4$ with increasing pump power, hence, one can expect further improvement of the laser characteristics. One can get the best results at the $BaWO_4$ orientation E//C4, and slightly poorer at E⊥C4. An even longer KGW crystal demonstrates a much higher threshold and considerably lower slope efficiency (about 45 %) in the same experimental scheme.

IR Raman shifting of the Nd:GGG solid-state laser fundamental wavelength $\lambda_L = 1062.1$ nm in the $BaWO_4$ crystalline Raman laser to the first Stokes wavelength $\lambda_{1St} = 1177.9$ nm was studied in [81,82]. Results of the pump-to-output conversion in the $BaWO_4$ Raman laser are shown in Fig. 4, which demonstrates the more than 30-% slope efficiency and the 15 mJ output energy with a megawatt peak power level for a 10 Hz repetition rate.

As we discussed above, application of the intracavity IR pumping scheme of a Raman laser can give an opportunity to increase the IR Raman conversion efficiency up to 100 % (by use of the nonlinear intracavity dumping regime), to improve the spatial beam quality (beam clean up), and to decrease the pulse duration with increasing peak power.

The Raman laser efficiency of the $SrWO_4$ SRS crystal was studied in [80] under similar conditions. The laser scheme differed from that considered above by a shorter cavity (70 mm), lower reflectivity of the output cou-

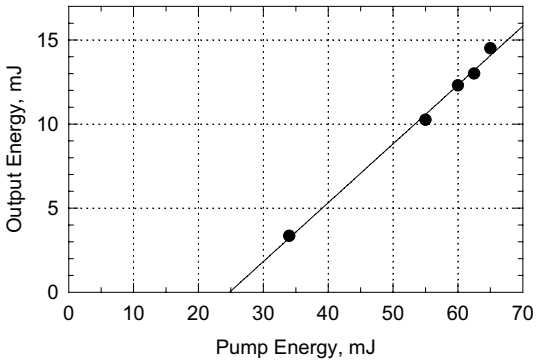

Fig. 4. The first Stokes (1179, 9 nm) output energy of a $BaWO_4$ Raman laser versus 1062.1 nm pump energy of a Nd:GGG laser

pler ($R_{1.05–1.32} = 30 \pm 5\,\%$), double the focal length of the focusing lens ($f = 100$ cm), and a twice larger focal spot ($\varnothing = 200\,\mu$m).

To prevent the coupling between the SRS crystal (without antireflection coatings), the Raman laser cavity, and the pump laser cavity, they were realigned to about 1° from each other.

Figure 5 shows the Raman laser output energy versus the pump energy for the new $SrWO_4$ and $BaWO_4$ crystals in comparison with KGW and $Ba(NO_3)_2$. One can see that the $SrWO_4$ crystal has a lower threshold and about twice the efficiency ($\approx 12\,\%$) than KGW. In spite of the poorer threshold, gain, and output characteristics of $SrWO_4$ in comparison with those

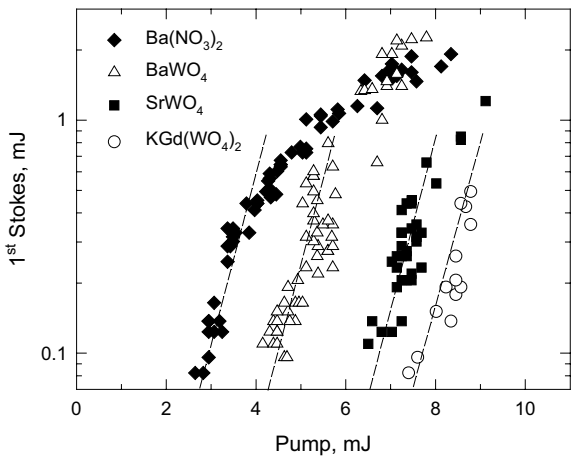

Fig. 5. Dependences of the first Stokes output energy on the pump energy for $Ba(NO_3)_2$ 49 mm long (*rhombs*), $BaWO_4$ 43 mm long (*triangles*), $SrWO_4$ 47 mm long (*squares*), and $KGd(WO_4)_2$ 50 mm long (*circles*) crystals

of $BaWO_4$ and $Ba(NO_3)_2$ crystals, the $SrWO_4$ crystal allows a rather high level of rare earth doping, which makes it promising for many applications as a multifunctional nonlinear (SRS) and active material.

The SRS self-conversion of laser radiation inside a Nd^{3+}:$SrWO_4$ laser crystal was first observed under flash lamp pumping in a Q-switched regime [80]. With cavity mirrors of high reflectivity at the fundamental wavelength of 1.06 μm, the first Stokes oscillation at 1.18-μm wavelength was recorded with an output energy of 3 mJ. The first Stokes oscillation of this Raman laser combined two oscillation mechanisms: the broadband stimulated emission of F_2^- color centers and the SRS inside the laser medium. This combination allowed SRS at lower intracavity energy density, i.e. reduced the SRS threshold.

8.1 Mid-IR $BaWO_4$ Raman Laser

An important advantage of barium tungstate crystals is their transparency in the much deeper IR region than the transparency of a $Ba(NO_3)_2$ high-gain Raman crystal. This could allow one to use these materials to develop a Raman laser for the mid-IR spectral region (from 2 to 5 μm), which is now one of the most interesting but hard-to-reach regions. The main problem here (besides the transparency) is that the Raman frequency shift of crystals is usually about 1000 cm^{-1}, hence to obtain mid-IR radiation one should start from as long pump wavelength as possible and use the second or even third Stokes of stimulated scattering. In addition, the Raman gain drops rapidly with longer wavelength of pumping.

An attempt to get Raman laser radiation with a longer wavelength was done in [83] using 1.34-μm pump radiation of an accousto-optically Q-switched Nd^{3+}:YAG laser. A 42-mm long $BaWO_4$ SRS crystal was placed in the cavity formed by a rear plain HR mirror with 90–100 % reflectivity for 1.5–2.0 μm spectral range and about 80 % transmittance at 1.34 μm pumping wavelength. The pump radiation was focused within the Raman laser cavity by a lens with a focal length of 120 mm.

The measured oscillation spectra of the $BaWO_4$ Raman laser for an output mirror with $R_{1.54} = 50\,\%$ and $R_{1.79} = 14\,\%$ reflectivity is shown in Fig. 6a. As can be seen, even for 50 % reflectivity at the first Stokes wavelength (1.53 μm), two additional peaks in the Raman laser output spectrum appear at the wavelengths of 1.79 μm (second Stokes) and 2.15 μm (third Stokes). Two low-intensity maxima near the oscillation lines of the first and second Stokes are associated with another weaker vibronic mode observed in the $BaWO_4$ spontaneous Raman and SRS spectrum with the frequency shift of 332 cm^{-1} [85].

Examples of input–output characteristics of the mid-IR Raman laser are shown in Fig. 6b. The total conversion slope efficiency from a 1.34-μm pump to the first 1.53 and second 1.79 μm Stokes wavelengths was about 22 %. In this regime, the conversion efficiency for the first and second Stokes radiation was about 10 % each. Latest improvement of this Raman laser provide up to

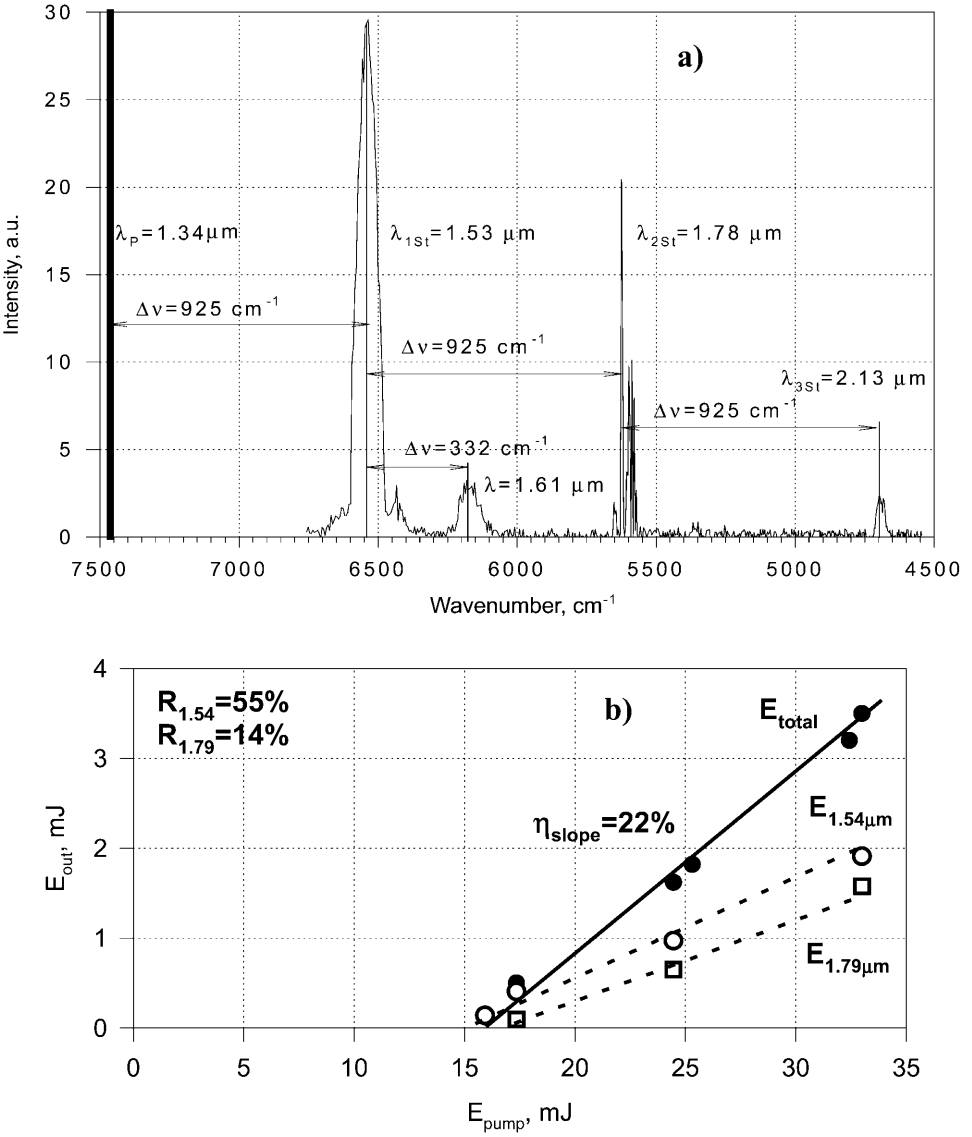

Fig. 6. Oscillation spectra of a $BaWO_4$ Raman laser pumped with a YAG:Nd Q-switched laser ($\lambda_P = 1.34\,\mu m$) (**a**) and input–output characteristics of a $BaWO_4$ Raman laser in a plane–plane cavity (**b**)

2.2 mJ of 1.7 μm radiation and 1.7 mJ of 2.1 μm radiation with slope efficiency till 14 % each.

8.2 Mid-IR Lasing in a Cr^{2+}:ZnSe Crystal with $BaWO_4$ Raman Laser Pumping

As was shown in the chapter on crystalline mid-IR lasers by Sorokina, Cr^{2+}-doped crystalline hosts such as ZnSe are very promising sources for tunable 2.1–2.7 μm mid-IR lasers. Cr^{2+}:ZnSe is very attractive due to its near unity fluorescence quantum efficiency at room temperature, high gain cross-section and wide vibronic absorption and emission bands. This crystal has been investigated under different pump sources in CW and pulsed operation. A diffusion Cr^{2+}-doped ZnSe crystal, 2.5 mm thick, was placed perpendicular relative to the pump and oscillation beams. The crystal demonstrated approximately 75 % absorption at the 1.53-μm pump wavelength. The Cr^{2+}:ZnSe laser cavity was about 50 mm long and was formed by an HR curved mirror with curvature of 100 mm and a plane output mirror with variable reflectivity. The 1.53-μm pump radiation was focused into the crystal by a lens with a focal length of 120 mm placed near the HR mirror of the Cr^{2+}:ZnSe laser cavity.

The input–output characteristics of the Cr^{2+}:ZnSe laser with different output mirror reflectivities are shown in Fig. 7a. As can be seen, the lasing threshold is about 200 μJ and the maximum slope efficiency is 11 %. The maximum total efficiency for the output mirror with $R = 34\,\%$ was determined to be about 8 %. The measured oscillation spectra of the Cr^{2+}:ZnSe laser are shown in Fig. 7b. The maxima of all the oscillation spectra are in the range 2.45–2.65 μm. The Cr^{2+}:ZnSe laser oscillation pulse width was measured to be about 7 ns, which is demonstrated in Fig. 7c and reflects the detector response time. Strong pulse shortening of Cr^{2+}:ZnSe oscillation is a characteristic feature of this regime and could be explained by gain switching in the active medium. As can be seen from Fig. 7c, the delay between the fronts of the pump and oscillation pulses is rather short (50 ns) and goes down to 25 ns with increasing output mirror reflectivity and pump energy.

9 $BaWO_4$ Picosecond Raman Frequency Shifters

A comparative study of picosecond stimulated Raman scattering in the new $BaWO_4$ crystal and in $KGd(WO_4)_2$ and $KY(WO_4)_2$ crystals was fulfilled in [86,87,88,89,90,91,92] for 28 and 40-ps pulses with a wavelength of 532 and 1064 nm, respectively. At visible, green light pumping, the picosecond Raman gain coefficient calculated for the $BaWO_4$ crystals from the pump threshold measurements by the formula $g_{\mathrm{exp}} = 25/I_{\mathrm{p}}l$, was equal to 14.4 cm/GW, which is 30 % higher than that for KGW (11.5 cm/GW) but 30 % lower then for KYW (18.7 cm/GW).

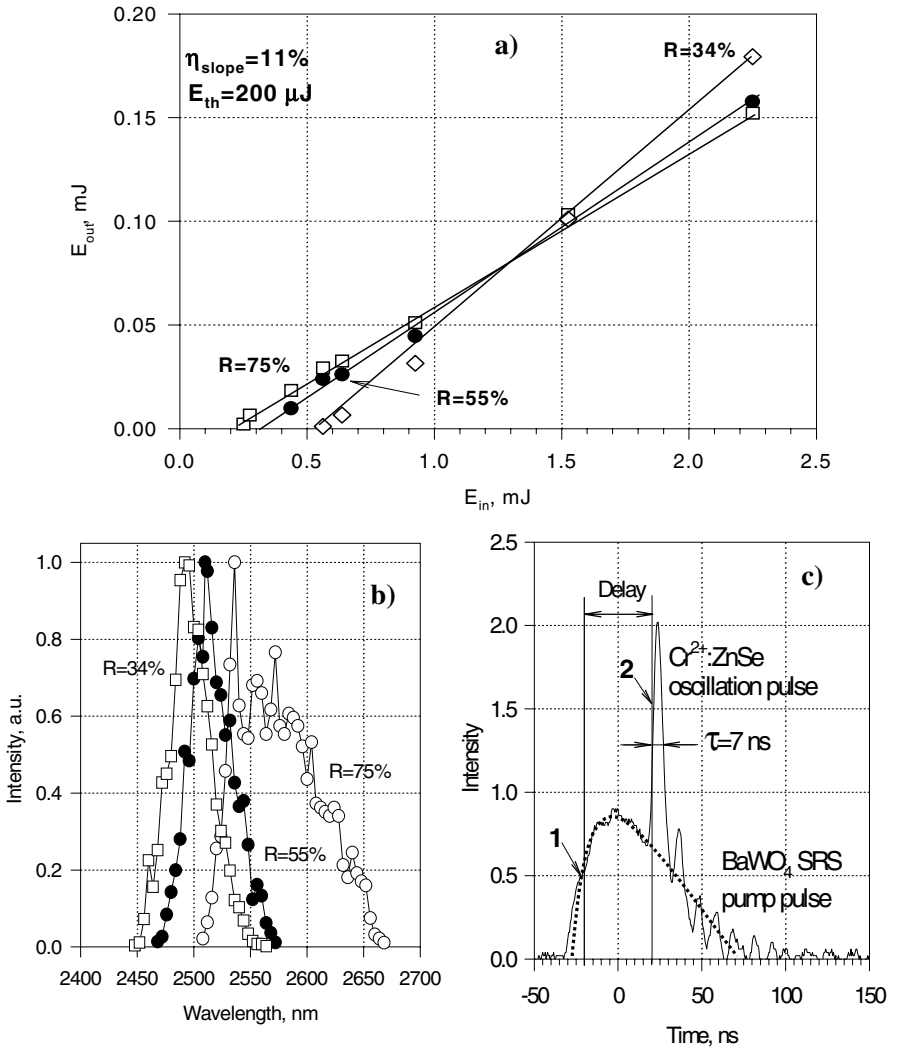

Fig. 7. Input–output characteristics of a Cr^{2+}:ZnSe laser (**a**), oscillation spectra of a Cr^{2+}:ZnSe laser with different output mirror reflectivities (**b**) and temporal shapes of $BaWO_4$ SRS pump (1) and Cr^{2+}:ZnSe laser oscillation (2) pulses for 55 % reflectivity of the output mirror at maximum pump energy (**c**)

In comparison with the steady-state regimes, where the $BaWO_4$ crystals show approximately 3 times higher gain than KGW, this ratio at picosecond pumping is moderate, though the $BaWO_4$ still has a higher gain than the KGW crystal. This is caused by the deeper transient behavior of $BaWO_4$ due to its smaller linewidth and longer dephasing time $T_R = 6.6$ ps of $BaWO_4$.

A much stronger difference can be found when comparing the $BaWO_4$ crystal with $Ba(NO_3)_2$. Under nanosecond pumping (steady-state regime), $BaWO_4$ has only a 20–30 % lower Raman gain (40 cm/GW against 52 cm/GW) [79,82]), but at the picosecond mode its gain is about three times higher (see Table 1).

For 1064-nm picosecond pumping, the $BaWO_4$ Raman gain reaches 3.8 cm/GW, which is slightly lower that for KYW (4.7 cm/GW), but higher than for KGW (3 cm/GW).

The maximum conversion efficiency for a 30-mm long $BaWO_4$ crystal under 532-nm picosecond pumping was 30 % for the first Stokes. This is much higher than the 18 % efficiency of an even longer (40 mm) KGW crystal. For the second Stokes scattering, both crystals show a similar efficiency of about 15 %.

The detailed study of $BaWO_4$ SRS under 1.06-μm, 50-ps pulsed pumping [91] allowed the authors to obtain the first Stokes radiation at 1180 nm with a conversion efficiency of 25 % in the single-pass and 35 % in the double-pass regimes. Placing a $BaWO_4$ crystal into the short (3.8 cm) cavity with an optimized output coupler provide an almost 100 % slope efficiency and 55 % pump-to-first-Stokes conversion efficiency with the output energy as high as 3 mJ (Fig. 8).

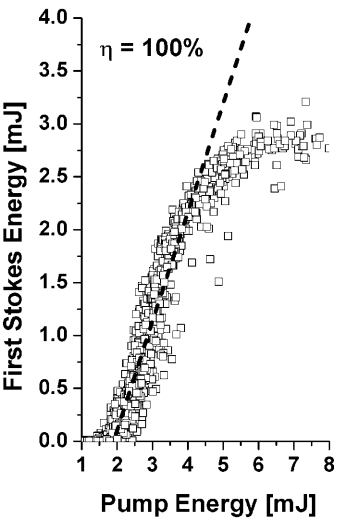

Fig. 8. The first Stokes (1180 nm) output energy of a picosecond $BaWO_4$ Raman laser with output coupler reflectivity $R = 33$ % and resonator length of 3.8 cm versus 1064-nm pump energy

Thus, we can conclude that $BaWO_4$ is the first universal crystal, which shows the almost record-high gain both under nanosecond and picosecond modes of operation.

10 $PbWO_4$ SRS Shifters and Raman Lasers

Another interesting SRS crystal was recently introduced to Raman laser development. This is a well known scintillating material, $PbWO_4$, with a scheelite structure similar to $BaWO_4$. Analogously to other tungstates, one can expect a high integral cross-section for the $PbWO_4$ crystal, but the measured linewidth of the totally symmetrical A_{1g} 904 cm^{-1} Raman vibration shows a rather high value of 5.6 cm^{-1} for a polycrystalline sample [75] close to KGW. Detailed study of the A_{1g} Raman line broadening at different temperatures up to the melting point shows that, similar to $CaWO_4$ and $SrWO_4$, lead tungstate $PbWO_4$ has a rather high Davydov splitting $\Delta E_{DS} = 32\,cm^{-1}$ caused by a strong $[WO_4]^{2-}$-$[WO_4]^{2-}$ intermolecular interaction [78]. This value is one or two orders of magnitude higher than ΔE_{DS} in $BaWO_4$ and $Ba(NO_3)_2$ crystals (with the record high peak value of gain) $\Delta E_{DS} =$ 0–1 cm^{-1}. The high density of acoustic phonon states leads to fast dephasing and large Raman line broadening $\Delta \nu_R(300\,K) = 4.7\,cm^{-1}$ (for single crystal) due to the direct relaxation processes between DS components with single-phonon absorption or emission.

The study of the $PbWO_4$ crystal by the picosecond SRS spectroscopy technique and under nanosecond Raman laser pumping was first reported in [93,94,95]. The authors presented the measured data on the gain coefficient (8.4 cm/GW at 532 nm and 3.1 cm/GW at 1064 nm) and some other characteristics of the $PbWO_4$ single crystal. They observed 18 different spectral lines of SRS Stokes and anti-Stokes radiation in the spectral region from 485.5 to 1117 nm under pumping by 1064-nm Nd:YAG laser pulses with a duration of 100 ps.

Raman laser oscillation of $PbWO_4$ crystals under external pumping by 100-ps pulses of a Nd:YAG laser at 1064 nm was studied in [93,94]. In the 200 mm long plane-concave laser cavity with spherical ($r = 0.5$ m) output coupling mirror with a reflectivity of 78 %, the first Stokes radiation energy of 1 mJ with slope efficiency as high as 40 % was obtained at the pump energy of 5 mJ. In those experiments, the pump beam was focused inside the 30 mm long $PbWO_4$ crystal by a lens with a focal length of 12 cm. There are also presented data on the steady-state Raman gain measured in visible light under pumping by 30-ps pulses of the frequency-doubled radiation of a Nd:YAG laser. The authors concluded that the gain coefficient of $PbWO_4$, measured to be 8.4 cm/GW, is slightly higher than 8 cm/GW of a KGW crystal, measured by the same technique.

IR Raman lasing by one or two 45-mm long $PbWO_4$ crystals was studied in a ring Raman laser cavity 285 mm long with two highly reflecting mirrors

and one output coupler with a reflectivity of 27 % for the first Stokes wavelength [95]. The Raman crystals were pumped by a Nd:YAG laser (1064 nm) beam 2.1 mm in diameter with a pulse duration of 7 ns. At the pumping energy of 36 mJ (close to the Raman crystal laser damage threshold), the output energy of the first Stokes radiation was as high as 5.3 mJ for one $PbWO_4$ crystal. The highest conversion efficiency reached 20 % for two SRS crystals in the cavity. The authors noted that the laser damage threshold for IR radiation was surprisingly low, at about 2 J/cm^2, which is less than half that for visible radiation.

The $PbWO_4$ crystal can also be easily activated by Nd^{3+} ions [93]. The first attempt to develop a diode-pumped passively Q-switched Nd^{3+}:$PbWO_4$ Raman laser with self-frequency conversion was described in [96]. An active and SRS Nd(0.5 at.%):$PbWO_4$ crystal with dimensions of $3 \times 3 \times 15\,mm^3$ was transversely pumped by a 100-W GaAlAs quasi-CW diode laser array ($\lambda = 808$ nm) with a pulse duration of 160 μs and a repetition rate of 20 Hz. In a high-reflective cavity 24 mm long, passively Q-switched by a Cr:YAG saturable absorber with $T = 95$ %, under a pump energy of 4.5 mJ, the Raman output energy at 1170 nm was rather low, at 2.5 μJ, with an efficiency of 0.6 % and threefold output pulse shortening to 8 ns.

11 Diode-Pumped CW Raman Fiber Lasers

Another class of highly efficient medium-power Raman lasers are CW single-mode Raman fiber lasers for the near and mid-infrared. The lasers can operate practically at any wavelength in the region from 1.1 to 1.6 μm with high-quality output power of several watts and are widely used for pumping optical fiber amplifiers.

Stimulated Raman scattering in a glass fiber was observed for the first time by *Stolen* et al. in 1971 [97]. The authors observed SRS in a single-mode glass fiber both as single-pass superradiant emission and as Raman oscillator output radiation. The great interest aroused after this pioneering work in the development of Raman fiber oscillators is explained by two of their advantages, namely, long interaction lengths in low-loss optical fibers and broad Raman gain bandwidth in glasses (extended to 500 cm^{-1}). In the late 1970s, low-threshold tunable Raman oscillators were created both for visible [98,99,100,101] and near-IR [102,103] regions. The development of high-quality low-loss fibers allowed one both to reduce the SRS threshold (below 1 W) and avoid the problems of fiber deterioration [99]. Laser radiation tunable within the spectral region from 5200 to 5600 A was obtained by using four orders of Stokes oscillation [101].

These results showed that laser diodes could be used for pumping Raman fiber oscillators. This promised the possibility of developing compact, efficient, and inexpensive sources of near infrared. But the problem was to achieve an efficient coupling of laser diode radiation to a single-mode fiber

core. This problem was solved by the development of double-clad fiber lasers (DCFL) pumped by laser diodes [104]. The authors suggested surrounding an Nd (Yb)-doped single-mode core by a layer with lower refractive index and thus form the core of a multimode waveguide. This structure was in turn surrounded by an outer cladding of still lower refractive index. This multimode structure guided the pump radiation around and through the central rare-earth-doped single-mode core. The shape and dimensions of the inner cladding were specifically chosen to provide efficient end-coupling for the output of high-power laser diode arrays. Such a scheme turned out to be very efficient for pumping Raman fiber lasers and later allowed the development of high-power (up to 35 W in CW mode) diffraction-limited fiber Nd (Yb)-doped lasers operating at around 1 μm (see for example [105,106,107]).

The principal elements of modern Raman fiber lasers are fiber Bragg gratings, serving as mirrors for different Stokes cavities. It was found that as many as six Raman Stokes can be obtained by using highly reflective in-fiber Bragg gratings [108]. In such a scheme, each intermediate Raman Stokes can be resonated and thereby efficiently converted to the next, higher Stokes until the cascade is terminated by a suitable output coupling for the desired Stokes order. Thus, in-fiber Bragg gratings allowed one to transform the multiresonant Raman fiber oscillator [101] into an elegant all-fiber structure.

The listed achievements served as a base for the development of Raman fiber lasers, which were required for pumping 1.3 μm Raman fiber amplifiers in the 1990s [109,110]. Further investigations showed that these lasers are also promising as pumping sources for other optical fiber amplifiers, including Er-doped fiber amplifiers. Wide applications of optical amplifiers in optical fiber communication systems, especially in WDM ones, stimulated active investigations of Raman fiber lasers. There were developed various types of efficient Raman fiber lasers, which were based on different fibers and had various Stokes frequency shifts, Stokes cavity designs, and pumping sources.

11.1 Raman Fiber Lasers Based on Germanosilicate Fibers

A widely used type of Raman fiber laser is based on well-developed, commercially available germanosilicate fibers. These fibers have high photosensitivity and thus allow writing Bragg gratings directly in them. The Raman scattering cross-section in germanosilicate fibers is higher than in silica fibers and increases (as well as the photosensitivity) with increasing Ge content.

For the first time, the third Stokes (1239 nm 300 mW CW) of a high Ge-doped fiber pumped by a 1060-nm Nd:YAG laser was used for pumping a 1.3-μm Raman fiber amplifier in [109]. The CW radiation of a diode-pumped germanosilicate Raman fiber laser for the same purpose was first obtained in [110] using a fiber 800 m long, which was H_2-sensitized to increase the photosensitivity. Three pairs of Bragg gratings forming the Stokes cavities were written directly in the germanosilicate fiber. The source of 1060-nm pumping was a diode-pumped Nd DCFL. With a 20 % output coupler, the

third Stokes radiation (1240 nm) had a threshold of 175 mW and a slope efficiency of 53 %.

A fifth-order cascaded Raman laser based on highly doped germanosilicate fiber was constructed in [108]. Five pairs of Bragg gratings were written in the H_2-sensitized fiber. The 1117-nm pump source was a diode-pumped Yb DCFL. With a 20 % output coupler, the authors obtained the fifth Stokes radiation (1484 nm) with a threshold of 660 mW, slope efficiency of 46 %, and output power of 1.5 W. The laser can be used to pump high-power and remotely pumped Er-doped fiber amplifiers.

Even more impressive results on fifth-order cascaded Raman fiber lasers were reported by *Innis* et al. [107]. The authors managed to obtain 1472-nm output radiation with a power of 8.5 W using pumping by a 20.5-W Yb double-clad fiber laser at 1101 nm.

Another way to construct cascaded Raman fiber lasers is to use fused WDM couplers instead of Bragg gratings to form Raman cavities. Such a cascaded Raman fiber laser operating at 1240 nm under pumping by a 1060-nm Yb fiber laser was developed on the base high Ge-doped fiber in [111]. In [112], also using high Ge-doped fiber as the active medium, a 1480-nm Raman fiber laser based on both a fused WDM coupler and Bragg gratings was developed. The efficiency of cascaded Raman lasers with fused WDM couplers turned out to be lower than that of lasers with Bragg gratings [107,108,110].

It should be noted that an essential drawback of Raman lasers based on germanosilicate fibers is the relatively small Raman frequency shift equal to about 440 cm^{-1}. The problem is that the best pumping sources for Raman fiber lasers operate in the vicinity of 1 μm, while the most desired output wavelength is 1450–1480 nm, which can be used for pumping optical amplifiers (Er-doped and Raman) operating in the 1.55-μm spectral window. Such a conversion can be obtained with six Stokes, i.e. it is necessary to write six pairs of Bragg gratings in a fiber, which makes the laser design too complicated and reduces the conversion efficiency.

To have efficient conversion, one should use Raman Stokes of lower orders, i.e. choose fibers with large Stokes shifts. In this connection, it should be noted that in the early 1980s researchers from AT&T Bell Laboratories constructed a Raman fiber laser for the 1.55-μm spectral region pumped by a 1060-nm Nd:YAG laser (see [113] and references therein). The active medium was molecular D_2 diffused into a l00-m long single-mode germanosilicate fiber. The Raman shift of D_2 is 2972 cm^{-1}, which allowed the authors to obtain laser radiation at 1560 nm. However, this fiber cannot be used in practice because it must be stored at liquid nitrogen temperature to prevent D_2 outdiffusion.

11.2 Phosphosilicate Fiber-Based Raman Lasers

A large Stokes shift can be obtained in phosphosilicate fibers, which show a strong Raman line shifted by 1330 cm^{-1} [114]. In addition, phosphosili-

cate fibers have rather high photosensitivity to permit writing Bragg gratings directly in them by 193-nm radiation [115]. However, phosphosilicate fibers have a grave drawback, specifically, phosphosilicate fibers containing more than 10 mol% of P_2O_5 have a high level of optical losses. Low-loss high P-doped fibers were suggested as active media Raman fiber lasers in [116]. In the first experiment [117], the radiation of phosphosilicate fiber pumped by a 1060-nm Nd:YAG laser was obtained at 1.24 and 1.48 μm for the first and second Stokes, respectively. These results demonstrated the high potential of Raman phosphosilicate fiber lasers.

Further improvements in the technology of phosphosilicate fibers resulted in reducing optical losses to a level below 1 dB/km for the spectral region from 1.2 to 1.6 μm [118]. As shown in [119], the phosphosilicate fiber Raman scattering spectrum (Fig. 9a) has a narrow line shifted by 1330 $cm^{-}1$, which relates to P=O bonds, and a broad band with the maximum at 490 cm^{-1}, which consists of overlapping SiO_2- and P_2O_5-related components. Hence, it is possible to construct Raman fiber lasers using the two frequency shifts, at 490 cm^{-1} and 1330 cm^{-1}, to get new wavelengths of laser radiation.

Efficient phosphosilicate fiber-based Raman lasers operating at wavelengths of 1240 nm were developed in [120,121]. The active phosphosilicate fiber of the Raman fiber laser pumped by a Nd fiber laser (1060 nm) contained 13 mol% of P_2O_5 ($\Delta n = 0.011$) and was 200 m long. To improve the fiber photosensitivity, the phosphosilicate fiber was loaded with hydrogen for four days under a pressure of 150 bars at a temperature of 50 °C. The gratings were written by an ArF excimer laser (193 nm) using a phase mask technique. The output power of the 1240 nm Raman fiber laser (Fig. 9b) reached a maximum of 2.3 W at a pump power of 3.5 W. The quantum efficiency was

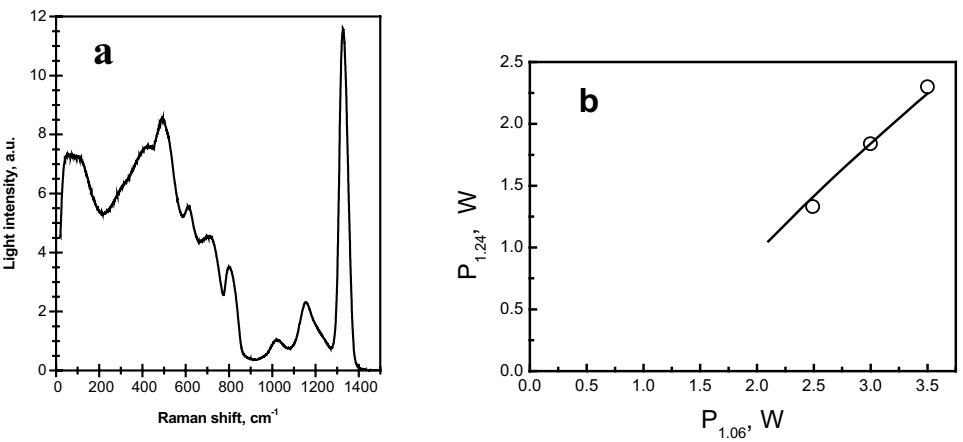

Fig. 9. (**a**) Raman spectrum of phosphosilicate fiber. (**b**) Output power of the 1.24-μm Raman laser versus 1.06-μm pump power: (*circles*) experimental points and (*solid line*) numerical simulation

77 %, which considerably exceeded the published data for the lasers based on germanosilicate fibers [110,111].

A 1.48-μm CW Raman fiber laser was developed in [122]. It consisted of a pigtailed LD array pump module, a Yb-doped double-clad fiber laser, and a 1.48-μm cascaded Raman converter (Fig. 10). The pump light is launched into the first cladding of the Yb fiber through a short piece of standard fiber (Flexcor 1060 with low-index polymer coating, length 1 cm) with a highly reflecting 1.06-μm Bragg grating written in the core. The piece of Flexcor 1060 fiber served as a multimode waveguide for the pump radiation. The output coupler of the Yb fiber laser was formed by a 5 % Bragg grating. The estimated mode field diameters (MFDs) of the Yb fiber and the standard fiber at 1.06 μm were 6.9 and 7.1 μm, respectively, and permitted splicing of these fibers (splicing points S2 and S3) with optical loss of 0.1 dB. The length of the Yb-doped double-clad fiber was 13 m, long enough to absorb the pump radiation at 976 nm. The mean diameter of the first cladding was 125 μm. The multimode pump was transformed into high-brightness 1.06-μm radiation with a slope efficiency of 80 %. The laser power was 3.3 W at the maximum LD array power of 4.5 W, which corresponds to a total light-to-light efficiency of 73 %.

The cascaded resonant Raman laser cavity was formed by two pairs of Bragg gratings with a phosphosilicate fiber between them. All the gratings were written in Flexcor fiber after H_2 preloading. The Raman laser gratings have reflectivity > 99 %, except the 1.48-μm output coupler, whose reflectivity was 15 %. A small nonresonant excess loss of approximately 0.1–0.15 dB was found in each of the two chains consisting of three Bragg gratings. The phosphosilicate fiber was 1 km long. The fiber core contained 13 mol% of phosphorous, yielding a refractive-index difference of 0.011. The optical losses of the fiber length were 1.7, 1.0, and 0.8 dB at 1.06, 1.24, and 1.48 μm, respectively. The P_2O_5-doped fiber had MFDs of 6.3 and 10.4 μm at 1.06 and 1.48 μm, whereas the corresponding MFDs in the Flexcor fiber were 7.1 and 12.7 μm, respectively. In spite of the mismatched MFDs, the authors managed to achieve optical losses as low as 0.05 dB by optimizing the splicing conditions (splices S4 and S5).

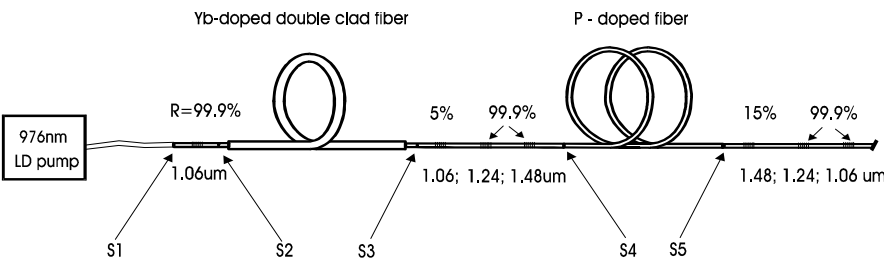

Fig. 10. Experimental setup of 1.48 μm two cascaded Raman laser pumped with a Yb-doped double-clad fiber laser

An important feature of the 1.48-μm Raman converter emission spectrum (Fig. 11a) is the absence of silica Stokes (440 cm^{-1}) peaks at 1.12 and 1.31 μm, hence rejection optical filters (such as long-period fiber gratings) for suppressing the silica Stokes peaks are not necessary.

The suppression of the 1.24-μm radiation corresponding to the first phosphorous Stokes order was 20 dB. The output power of the second-order phosphosilicate Stokes is shown in Fig. 11b. The first Stokes radiation had a threshold of about 0.7 W and increased until the pump power reached the second Stokes threshold (1.5 W); then, the first Stokes power was fixed at a level of 10 mW. The slope efficiency of the 1.48-μm second Stokes radiation with respect to the LD array power was 34 %. The maximum output power was 1 W (at a pump power of 4.5 W), and the spectral width was 0.75 nm (FWHM). Real efficiency could be further improved by reducing the Raman cavity loss.

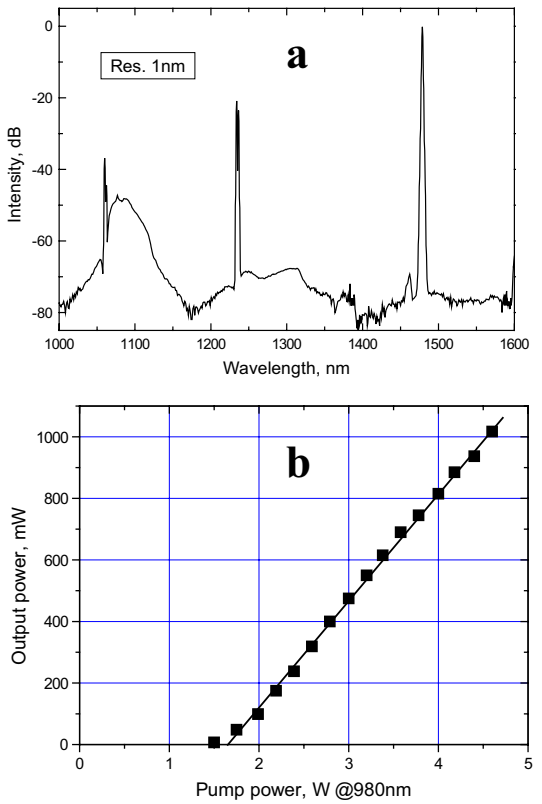

Fig. 11. (**a**) Emission spectrum of the 1.48-μm phosphosilicate fiber Raman converter. (**b**) Second-order Stokes 1.48-μm output power versus pump power

Raman lasers based on phosphosilicate fibers using 1330 and 490-cm^{-1} Stokes frequency shifts were developed in [123,124]. The two Raman bands with considerably different frequencies provide more possibilities of generating new laser wavelengths. With a tunable Yb double-clad fiber laser as a pump source, it is possible to obtain any wavelength in the spectral region from 1.1 to 1.6 μm with only three cascades of Raman conversion. The authors of [123,124] suggested Raman fiber lasers operating at 1407 and 1430 nm, which can be used, respectively, for pumping I500-nm Raman fiber amplifiers and in medical devices.

The authors used a 25-m Nd-doped fiber as the pump source and a specially developed P-doped silica fiber 975 m long as the Raman active fiber of the 1407-nm laser. It is important that the active fiber had relatively low optical losses at the wavelength of 1.4 μm associated with OH groups (1.1 dB/km). The Raman gain properties of a fiber can be characterized by the fiber Raman gain coefficient $g_0 = G_R/A_{eff}$ (in dB/km W), where G_R is the mean Raman gain coefficient of the core material (usually expressed in m/W) and A_{eff} is the effective area of the fiber core. Unlike G_R and A_{eff}, g_0 can be measured directly for each fiber ([101,121]).

The fiber Raman gain coefficient for the 1407-nm laser were measured to be $g_0(1.3\,\mu m/1.24\,\mu m) = 5.4\,dB/(km \cdot W)$ (SiO_2-related Stokes) and $g_0(1.24\,\mu m/1.06\,\mu m) = 6.8\,dB/(km \cdot W)$ (P_2O_5-related Stokes). The close values of these Raman gain coefficients enabled the authors to use the generation of both SiO_2- and P_2O_5-related Stokes components.

The Raman fiber laser had three optical cavities for the three successive Stokes wavelengths $\lambda_{S1} = 1236$ nm, $\lambda_{S2} = 1316$ nm, and $\lambda_{S3} = 1407$ nm. Here λ_{S1} corresponds to the P-associated Stokes shift of 1330 cm^{-1}, λ_{S2} and λ_{S3} to the SiO_2-associated Stokes shift of 490 cm^{-1}. Hence, the successive generation of Stokes components of both fiber core constituents (P_2O_5 and SiO_2) was used. The fiber laser cavities were formed by the pairs of fiber Bragg gratings, written in the germanosilicate fiber and spliced with the Nd-doped and P-doped fibers.

Figure 12a shows the output spectrum of this Raman laser. The dependence of the third Stokes output power (λ_{S3}) on the pump power (λ_P) is shown in Fig. 12b. The 1047-nm radiation had a linewidth of 0.5 nm and laser slope efficiency of 35 %. This efficiency can be considered high enough taking into account that the generation wavelength $\lambda = 1407$ nm coincides with the maximum of OH absorption in the fiber, which leads to high losses in the Raman cavity.

A similar laser scheme with a 1.089-nm Yb DCFL pumping laser was used for a laser operating at the wavelength of 1430 nm. Such lasers are very promising for medical applications because their wavelength coincides with a water absorption band. The RFL output power at 1430 nm was 1.4 W.

Long wavelength 1.65-μm operation of two stage fiber Raman lasers on phosphosilicate and germanosilicate fibers with output power as high as

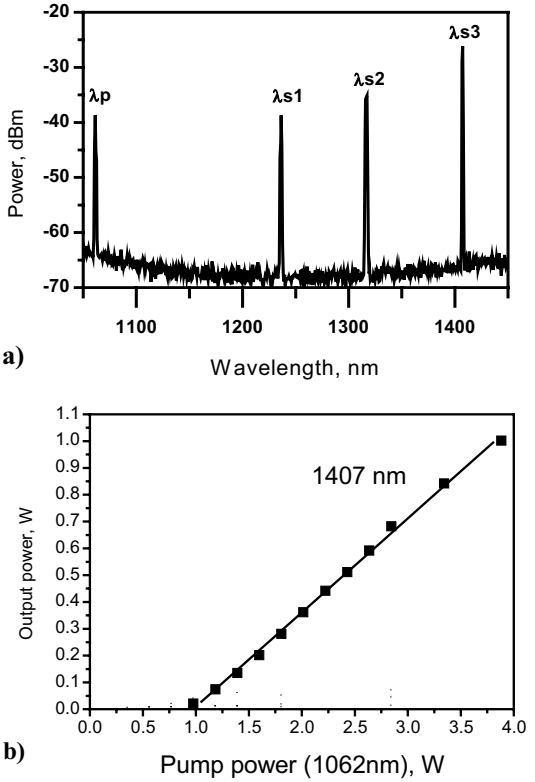

Fig. 12. (**a**) Output spectrum and (**b**) output power of the 1407-nm phosphosilicate fiber Raman laser under pumping by a Nd fiber laser

1.2 W and conversion efficiency 15 % was realized in [125] under LD pumped Yb fiber laser pumping.

Thus, CW Raman fiber lasers pumped by Yb (Nd) double-clad fiber lasers can operate in the spectral region from 1.1 to 1.6 μm with single-mode output power of 1–10 W, spectral bandwidth of radiation of about 1 nm, and conversion efficiency close to 50 %.

At present the main application of Raman fiber lasers is the pumping of Raman and Er-doped amplifiers.

Using higher power Yb (Nd) DCFL for pumping it is possible to obtain an output power of several tens of watts. Due to the high brightness and quality of output beams and the possibility of choosing generation wavelengths, Raman fiber lasers can also find wide applications in material processing, printing, marking, medicine, and free space optical communication.

12 Conclusion

We have demonstrated the wide potentialities of synthetic optical SRS crystals and glass optical fibers and methods of research and development. The large size and high optical quality of synthesized single crystals and fibers with various nonlinear parameters, transparency ranges, and Raman frequencies and linewidths give the opportunity to develop a great variety of solid-state Raman lasers and shifters. Application of stimulated Raman scattering in crystals and fibers extends the spectral range, improves the beam quality, and decreases the pulse width of pump laser radiation. SRS solid-state laser technology is especially important for the mid-IR spectral region, where the development of directly oscillating crystalline lasers with population inversion runs into the problems caused by fast multiphonon relaxation and decreasing quantum yield. A number of crystals and glasses transparent in the mid-IR and with high cubic optical nonlinearity can provide a step-by-step SRS shift of radiation frequency of existing tunable lasers (e.g. Cr:ZnSe 2–3 μm lasers, see the chapter by Sorokina in this volume) to the longer mid-IR region.

Acknowledgements

This work was partially supported by the International Science and Technology Center and European Office of Aerospace Research and Development (Partner project #2022p).

References

1. E. J. Woodbury, W. K. Ng: Excitation of a ruby oscillator in a near infrared region, Proc. IRE **50**, 2367 (1962) 351
2. C. V. Raman, K. S. Krishnan: A new type of secondary emission, Nature (London) **121**, 501 (1928) 351
3. G. S. Landsberg, L. I. Mandel'shtam: A new phenomenon of light scattering, Zh. Rus. Fiz. Khim. Obshch. **60**, p. 335 (1928) 351
4. G. Placzek: *Rayleigh-Streuung und Raman Effect*, in Handbuch der Radiologie **6**, 2, 2. Auflage (Leipzig 1934) 351, 352
5. R. W. Hellwarth: Theory of stimulated Raman scattering, Phys. Rev. **130**, 1850 (1963) 351, 352
6. V. A. Zubov, M. M. Sushchinskii, I. K. Shuvalov: Stimulated Raman scattering of light, Usp. Fiz. Nauk **83**, 197 (1964) (in Russian) [Engl. transl. Sov. Phys. Usp., 7419 (1964)] 351
7. G. Eckhart: Selection of Raman laser materials, IEEE J. Quantum Electron. **2**, (1966) 351, 370
8. N. Bloembergen: The stimulated Raman effect, Am. J. Phys. **35**, 989 (1967) 351, 352
9. R. Loudon: The Raman effect in crystals, Adv. Phys. **13**, 423 (1967) 351, 352

10. V. N. Lugovoi: *Vvedenie v Teoriyu Vynuzhdennogo Kombinalsionnogo Rasseyaniya* (Moscow, Nauka 1968) (in Russian) [Introduction to the Theory of Stimulated Raman Scattering] 351, 352
11. A. Glass: Design consideration for Raman lasers, IEEE J. **3**, 11, 516–520 (1967) 351
12. W. Kaiser, M. Maier: Stimulated Rayleigh, Brillouin and Raman scattering, in *Laser Handbook*, F. T. Arecchi, E. O. Shultz-Dubois (Eds.) (North-Holland, Amsterdam 1972) p. 1077 351, 353
13. A. Z. Grasyuk: Raman lasers, Kvantovaya Elektron. **3**, 485 (1974) (in Russian) [Sov. J. Quantum Electron.] 351, 353, 354
14. Yu. E. D'yakov, S. Yu. Nikitin: Stimulated Raman scattering, Kvantovaya Elektron. **14**, (10) 1925 (1987) (in Russian) [Sov. J. Quantum Electron.] 351
15. T. T. Basiev, R. C. Powell: Introduction to the special issue on solid-state Raman lasers, Opt. Mater. **11**, 301 (1999) 351, 354, 362
16. T. T. Basiev: Spectroscopy of new Raman-active crystals and solid-state Raman lasers, Physics Uspekhi **42**, 1051–1056 (1999) 351, 354, 362
17. P. G. Zverev, T. T. Basiev, A. M. Prokhorov: Stimulated Raman scattering of laser radiation in Raman crystals, Opt. Mater. **11**, 335 (1999) 351, 354, 362
18. R. C. Powell, T. T. Basiev: Seventy years of Raman scattering, in *Advances in Laser Physics*, V. S. Letokhov, P. Meystre (Eds.) (Harwood Academic, Amsterdam 2000) pp. 55–66 351, 354, 355, 362
19. L. I. Belevtseva, V. N. Voitsekhovskii, N. A. Nazarova, G. I. Romanova, M. V. Shvedova, V. E. Yakobson: Basic properties of barium nitrate optical crystals, Opt. Mekh. Promst. **56**, 38 (1989) (in Russian)
V. N. Voitsekhovskii, S. M. Karpukhin, V. E. Yakobson: Single crystal barium nitrate and sodium nitrate as efficient materials for laser radiation frequency conversion based on stimulated Raman scattering, J. Opt. Tech. **62**, 770–776 (1995) 351, 354, 355
20. P. G. Zverev, T. T. Basiev, V. V. Osiko, A. M. Kulkov, V. N. Voitsekhovskii, V. E. Yakobson: Physical, chemical and optical properties of barium nitrate Raman crystal, Opt. Mater. **11**, 315–334 (1999) 351, 354, 355, 369
21. V. A. Berenberg, S. N. Karpukhin, I. V. Mochalov: Nonlinear optics of laser crystal of potassium gadolinium tungstate activated with neodymium Nd^{3+}:$KGd(WO_4)_2$, Kvantovaya Elektron. **14**, 1849 (1987) (in Russian) [Engl. transl. Sov. J. Quantum Electron. **17**, 1178 (1987)] 354, 355
22. I. V. Mochalov: Nonlinear optics of laser crystal of potassium gadolinium wolframate activated with neodymium $KGd(WO_4)_2$:Nd^{3+}, Optich. Zhurn. **11**, 4 (1995) 354, 355
23. A. S. Eremenko, S. N. Karpukhin, A. I. Stepanov: Stimulated Raman scattering of the neodymium laser second harmonic in nitrate crystals, Kvantovaya Elektron. **7**, 196–197 (1980) (in Russian) [Engl. transl. Sov. J. Quantum Electron. **10**, 113 (1980)] 355
24. S. N. Karpukhin, A. I. Stepanov: Stimulated emission from the cavity under SRS in $Ba(NO_3)_2$, $NaNO_3$, and $CaCO_3$ crystals, Kvant. Elektr. **13**, 1572–1577 (1986) (in Russian) [Sov. J. Quantum Electron.] 355, 356
25. S. A. Vitsinskii, V. K. Isakov, S. M. Karpukhin, L. L. Lovchil: Stimulated Raman scattering of copper-vapor laser radiation in barium nitrate crystal, Kvant. Elektr. **20**, 1555–1558 (1993) (in Russian) [Sov. J. Quantum Electron.] 355, 356

26. S. N. Karpukhin, V. E. Yashin: Generation and amplification of Raman emission in crystals, Kvantovaya Elektron. **10**, 1992 (1984) (in Russian) [Sov. J. Quantum Electron. **14**, 1337 (1984)] 355, 357
27. V. N. Voitsekhovskii, S. N. Karpukhin, V. E. Yakobson: Barium nitrate and sodium nitrate single crystals as efficient materials for Raman conversion, Opt. Zhurn. **Ll**, 30–37 (1995) 355, 357
28. P. G. Zverev, J. T. Murray, R. C. Powell, R. J. Reeves, T. T. Basiev: Nonlinear optics of laser crystal of potassium gadolinium wolframate activated with neodymium $KGd(WO_4)_2$:Nd^{3+}, Opt. Commun. **97**, 59–64 (1993) 357
29. T. T. Basiev, Yu.K. Voron'ko, S. B. Mirov, V.V, Osiko, A. M. Prokhorov: Tunable solid-state lasers based on color centers in ionic crystals, Izv. Akad. Nauk SSSR, Ser. Fiz. **46**, 8, 1600–1610 (1982) (in Russian) 357
30. T. T. Basiev: Tunable color-center lasers and their application in selective spectroscopy of disordered media, Izv. Akad. Nauk SSSR, Ser. Fiz. **49**, 68–77 (1985) (in Russian) [Bull. Sov. Acad. Sci. USSR Phys. Ser.] 357
31. T. T. Basiev, V. V. Osiko, S. B. Mirov: Room-temperature color center lasers, IEEE J. Quantum Electron. **24**, 1052 (1988) 357
32. T. T. Basiev, S. B. Mirov: *Room Temperature Tunable Color Center Lasers* (Gordon, Breach, New York 1994) 357, 358
33. T. T. Basiev, V. N. Voitsekhovskii, P. G. Zverev, F. V. Karpushko, A. V. Lyubimov, S. B. Mirov, V. P. Morozov, I. V. Mochalov, A. A. Pavlyuk, G. V. Sinitsyn, V. E. Yakobson: Conversion of tunable radiation from a laser utilizing an LiF crystal containing F_2^- color centers by stimulated Raman scattering in $Ba(NO_3)_2$ and $KGd(WO_4)_2$ crystals, Kvantovaya Elektron. **14**, 2452–2453 (1987) (in Russian) [Engl. transl. Sov. J. Quantum Electron. **17**, 1560–1561 (1987)] 357, 358, 366
34. T. T. Basiev, P. G. Zverev, F. V. Karpushko, V. A. Konyushkin, S. M. Kulashchik, S. B. Mirov, V. P. Morozov, V. S. Motkin, A. G. Papashvili, N. A. Saskevich, G. V. Sinitsyn, V. V. Fedorov: Lasing characteristics of tunable color center lasers, MALSAN 2000, Izv. Akad. Nauk SSSR, Ser. Fiz. **54**, 1450–1455 (1990) (in Russian) 358
35. P. G. Zverev, T. T. Basiev: Compact SRS laser on barium nitrate crystal, Proc. All-Union Conf. Opt. Las. **2**, Leningrad (1993) p. 363 (in Russian) 358, 359
36. P. G. Zverev, T. T. Basiev: Barium nitrate Raman laser, J. Phys. IV (Paris) **4**, C4–599 (1994) 358, 359
37. P. G. Zverev, T. T. Basiev, A. M. Prokhorov: Barium nitrate lasers operating in the near IR spectral region, CLEO/Europe'94, Tech. Digest (1994) paper 94TH0614-8, p. 154 358, 359
38. P. G. Zverev, T. T. Basiev, I. V. Ermakov, A. M. Prokhorov: Stimulated Raman scattering in barium nitrate crystal in an external optical cavity, in *Laser Methods of Surface Treatment and Modification*, Proc. SPIE **2498**, 164 (1994) 358, 359
39. T. T. Basiev, V. B. Sigachev, M. E. Doroshenko, P. G. Zverev, V. V. Osiko, A. M. Prokhorov: Crystalline passive Q-switching of 1.3 μm Nd-lasers and Raman shifting to eye-safe region, CLEO/Europe'94, Tech. Digest (1994) paper 94TH0614-8, p. 125 358, 359
40. T. T. Basiev, V. B. Sigachev, M. E. Doroshenko, P. G. Zverev, V. V. Osiko, A. M. Prokhorov: Passive Q-switching of 1.3 μm Nd-lasers with Nd^{2+}:SrF_2 and V^{3+}:YAG crystalline saturable absorbers and application to Raman shifting

to eye-safe region, in *Laser Methods of Surface Treatment and Modification*, Proc. SPIE **2498**, 171 (1994) 358, 359
41. P. G. Zverev, T. T. Basiev: Barium nitrate Raman laser for near IR spectral region, *OSA Trends Opt. Photonics Adv. Solid-State Lasers* **24**, 288, B. H. T. Chai, S. A. Payne (Eds.) (Opt. Soc. Am., Washington, DC 1995) 358, 359
42. P. G. Zverev, T. T. Basiev, V. Jia, H. Liu: Raman spectroscopic and nonlinear optical properties of barium nitrate crystal, OSA Trends Opt. Photonics Adv. Solid-State Lasers **1**, 554, S. A. Payne, C. Pollok (Eds.) (Opt. Soc. Am., Washington, DC 1996) 358, 359
43. J. T. Murray, W. L. Austin, R. C. Powell, N. Peyghambarian: Theory of Raman gain spectrum transformation, Opt. Mater. **11**, 373 (1999) 359
44. J. T. Murray, R. C. Powell, E. L. Austin: High brightness, eye-safe lasers, Opt. Photon. News **6**, 32 (1995) 360
45. J. T. Murray, R. C. Powell, N. Peyghambarian, D. Smith, W. Austin, R. A. Stolzenberger: Generation of 1.5 µm radiation through intracavity solid-state Raman shifting in $Ba(NO_3)_2$ nonlinear crystals, Opt. Lett. **20**, 1017–1019 (1995) 360
46. J. T. Murray, W. L. Austin, L. K. Calmes, R. C. Powell, G. J. Quarles: Nonlinear cavity-damped intracavity solid state Raman laser transmitters, in OSA Trends Opt. Photonics Adv. Solid-State Lasers **20**, 72–76, S. A. Payne, C. K. Pollock (Eds.) (Opt. Soc. Am., Washington, DC 1996) 360
47. E. O. Ammann, C. D. Decker: Raman spectroscopic and nonlinear optical properties of barium nitrate crystal, J. Appl. Phys. **48**, 1973–1975 (1977) 361
48. E. O. Ammann: High average power Raman oscillator employing a shared resonator configuration, Appl. Phys. Lett. **32**, 52–54 (1978) 361
49. G. G. Grigoryan, S. B. Sogomonyan: A synchronously pumped picosecond SRS-laser on a $LiIO_3$ crystal, Kvantovaya Electronika **16**, 2180–2183 (1989) [Sov. J. Quantum Electron.] 361
50. H. M. Pask, J. A. Piper: Practical 580-nm source based on frequency doubling of an intracavity-Raman-shifted Nd:YAG laser, Opt. Commun. **148**, 285–288 (1998) 362
51. H. M. Pask, J. A. Piper: Efficient all-solid-state yellow laser source producing 1.2 W average power, Opt. Lett. **24**, 1490–1492 (1999) 362
52. M. Revermann, H. M. Pask, Justin L. Blows, T. Omatsu: Thermal lensing measurements in an intracavity $LiIO_3$ Raman laser, in OSA Trends Opt. Photonics Adv. Solid-State Lasers **34**, 506–509, H. Injeyan, U. Keller, Ch. Marshal (Eds.) (Opt. Soc. Am., Washington, DC 2000) 362
53. H. M. Pask, J. A. Piper: Diode-pumped $LiIO_3$ intracavity Raman laser, IEEE J. Quantum Electron. **36**, 949–855 (2000) 362
54. H. M. Pask, J. A. Piper: Design and operation of an efficient 1.4 W diode-pumped Raman laser at 578 nm, in Tech. Digest, Int. Conf. Adv. Solid-State Lasers, Quebec, Canada, Feb. 2002 (Opt. Soc. Am., Washington, DC 2002) WD1 362
55. K. Andryunas, Yu. Vishakas, V. Kabelka, I. V. Mochalov, A. A. Pavlyuk, G. T. Petrovskii, V. Syrus: Raman self-conversion of Nd^{3+} laser radiation in crystals of double tungstates, Pis'ma v Zhurnal Eksperi Teor. Fiz. **42**, 333 (1985) (in Russian) [Engl. transl. JETP Lett. **42**, 410–412 (1986)]
K. Andryunas, Yu. Vishakas, V. Kabelka, I. V. Mochalov, A. A. Pavlyuk, N. V.

Ionina, V. Syrus: A method of generation of picosecond pulses at a Raman frequency, USSR patent no. 1227074 (1984) (in Russian) 362, 364
56. A. M. Ivanyuk, M. A. Ter-Pogosyan, P. A. Shakhverdov, V. D. Belyaev, V. L. Ermolaev, H. P. Tikhonova: Picosecond radiation pulses at intracavity stimulated Raman scattering inside the active element of neodymium laser, Optika i Spectrosk. **59**, 950–952 (1985) (in Russian) [Sov. Opt. Spectrosc.] 364
57. A. V. Mikhailov, I. V. Mochalov, A. V. Lyubimov: Raman scattering in KGW crystals, in *Lasers and Optical Nonlinearity*, E. K. Maldutis (Ed.) (Vilnyus, 1987) pp. 265–269 (in Russian) 364
58. K. Andryunas, A. Barila, Yu. Vishchakas, V. Syrus: Investigation of pulse duration dynamics in a laser based on $KGd(WO_4)_2$:Nd^{3+} and $KY(WO_4)_2$:Nd^{3+} in *Lasers and Optical Nonlinearity*, E. K. Maldutis (Ed.) (Vilnyus, 1987) pp. 43–50 (in Russian) 365
59. K. Andryunas, A. Barila, Yu. Vishchakas, I. V. Mochalov, G. T. Petrovskii, V. Syrus: Temporal characteristics of picosecond pulses of SRS self-conversion, Optika i Spektroskopiya **64**, 397–401 (1988) (in Russian) [Sov. Opt. Spectrosc.] 365
60. Yu. K. Vishchakas, I. V. Mochalov, A. V. Mikhailov, R. F. Klevtsova, A. V. Lyubimov: Crystal structure and Raman scattering in $KGd(WO_4)_2$ crystals, Lietuvos fizikos rinkinys **28**, 224–234 (1988) 365, 370
61. I. V. Mochalov: Laser and nonlinear properties of the potassium gadolinium tungstate laser crystal $KGd(WO_4)_2$:Nd^{3+} (KGW:Nd), Opt. Eng. **36**, 1660–1669 (1997) 365
62. A. M. Ivanyuk, V. A. Sandulenko, M. A. Ter-Pogosyan, P. A. Shakhverdov, V. G. Chervinskii, A. V. Lukin, V. L. Ermolaev: Intracavity stimulated Raman scattering in a nanosecond neodymium laser based on potassium-gadolinium tungstate, Opt. Spektrosc. **62**, 961–962 (1987) (in Russian) []Sov. Opt. Spectrosc.] 366
63. V. A. Berenberg, S. N. Karpukhin, I. V. Mochalov: SRS of nanosecond pulses in $KGd(WO_4)_2$ crystals, Kvantovaya Electronika **14**, 1849–1850 (1987) (in Russian) [Sov. Quant. Electron.] 366
64. A. A. Kaminskii, N. S. Ustimenko, A. V. Gulin, S. N. Bagaev, A. A. Pavlyuk: Raman-parametric interactions in monoclinic $KGd(WO_4)_2$ and $KY(WO_4)_2$:Nd^{3+} crystals: picosecond multicomponent Stokes and anti-Stokes generation and nanosecond self-SRS conversion in human eye-safe 1.5 µm range, Dokl. Akad. Nauk **359**, 179–183 (1998) (in Russian) [Sov. Phys. Docl.] 367
65. N. S. Ustimenko, A. V. Gulin: 1.538 µm wavelength radiation of $KGd(WO_4)_2$:Nd^{3+} lasers based on stimulated Raman scattering with self-conversion, Pribory i Tekhnika Eksperimenta. **3**, 99–101 (1998) (in Russian) [Sov. Instr. Exp. Techn.] 367
66. J. Fideisen, N. J. Eichler, P. Peuser: Self-stimulating, transversely diode pumped Nd:$KGd(WO_4)_2$ Raman laser, Opt. Commun. **181**, 129–133 (2000) 367
67. A. A. Lagatsky, A. Abdolvand, N. V. Kuleshov: Passive Q-switching and self-frequency Raman conversion in a diode-pumped Yb: $KGd(WO_4)_2$ laser, Opt. Lett. **25**, 616–618 (2000) 367
68. A. S. Grabtchikov, A. N. Kuzmin, V. A. Lisinetskii, V. A. Orlovich, A. A. Demidovich, N. V. Eichler, A. Bednarkiewics, W. Strek, A. N. Titov: Yb:KGW

microchip laser performance: fundamental frequency generation and Raman self-frequency conversion, in Tech. Digest, Int. Conf. Adv. Solid State Lasers, Quebec, Canada, Feb. 2002 (Opt. Soc. Am., Washington, DC 2002) WB 6 367
69. T. T. Basiev, E. M. Dianov, E. A. Zakhidov, A.Ya. Karasik, S. B. Mirov, A. M. Prokhorov: Selective nonlinear spectroscopy of inhomogeneously-broadened phonon resonances in disordered medium, Pis'ma Zh. Eksp. Tear. Fiz. **37**, 192 (1983) (in Russian) [Engl. transl. JETP Lett. 37229 (1983)] 368
70. P. G. Zverev, T. T. Basiev: Study of line broadening of Raman-active vibration in barium nitrate crystal by the method of two-photon Raman gain spectroscopy, Kvantovaya Elektron. **22**, 12, 1241 (1995) (in Russian) [Sov. J. Quantum Electron.] 368, 369
71. P. G. Zverev, W. Jia, H. Liu, T. T. Basiev: Vibrational dynamics of the Raman-active mode in barium nitrate crystal, Opt. Lett. **20**, 2378 (1995) 368, 369
72. T. T. Basiev, A. A. Sobol, P. G. Zverev, Yu. K. Voron'ko, V. V. Osiko, R. C. Powell: Comparative Raman spectroscopy study of crystals for Raman lasers, in OSA Trends Opt. Photonics Adv. Solid-State Lasers **19**, 546, W. R. Rosenberg, M. M. Fejer (Eds.) (Opt. Soc. Am., Washington, DC 1998) 369
73. T. T. Basiev, A. A. Sobol, P. G. Zverev, V. V. Osiko, R. C. Powell: Comparative spontaneous Raman spectroscopy of crystals for Raman lasers, Appl. Opt. **38**, 594 (1999) 369, 370
74. T. T. Basiev, A. A. Sobol, P. G. Zverev, L. I. Ivleva, V. V. Osiko, R. C. Powell: Raman spectroscopy of crystals for stimulated Raman scattering, Opt. Mater. **11**, 307 (1999) 369, 370
75. T. T. Basiev, A. A. Sobol, P. G. Zverev, V. V. Fedorov, M. E. Doroshenko, L. I. Ivleva, N. M. Polozkov, V. V. Osiko, A. M. Prokhorov, G. Hager: Raman spectroscopy of tungstate crystals for Raman lasers, in *Laser '98*, V. J. Corcoran, T. A. Goldman (Eds.), Proc. Int. Conf. Tucson, Dec. 1998 (SRS, McLean, VA 1999) p. 712 369, 371, 379
76. T. T. Basiev, P. G. Zverev, A. A. Sobol, V. V. Fedorov, M. E. Doroshenko, V. V. Skornyakov, L. I. Ivleva, V. V. Osiko: Perspectives of tungstate crystals for Raman lasers, in *Novel Lasers and Devices – Basic Aspects*, Tech. Digest CLEO/Europe Focus Meeting 1999, Munich (2001) p. 160 369, 371
77. T. T. Basiev, A. A. Sobol, P. G. Zverev, L. I. Ivleva, V. V. Osiko: Laser material for stimulated Raman scattering, Russian patent no. 2178938 (27.01.2002, C1 Bull N3) 370, 371
78. T. T. Basiev, A. A. Sobol, Yu.K. Voron'ko, P. G. Zverev: Spontaneous Raman spectroscopy of tungstate and molybdate crystals for Raman lasers, Opt. Mater. **15**, 205–216 (2000) 370, 371, 379
79. P. G. Zverev, T. T. Basiev, A. A. Sobol, V. V. Skornyakov, L. I. Ivleva, N. M. Polozkov, V. V. Osiko: Stimulated Raman scattering in alkaline-earth tungstate crystal, J. Quantum Electron. **30**, 55–59 (2000) 371, 372, 378
80. T. T. Basiev, P. G. Zverev, A. A. Sobol, V. V. Osiko: Search and charcterization of new crystals for Raman lasers, in Tech. Digest Adv. Solid State Lasers (Opt. Soc. Am., Washington, DC 2002) MB 10 371, 372, 374
81. T. T. Basiev, N. E. Doroshenko, P. G. Zverev, A. M. Prokhorov: Solid-state laser of yellow spectral region, Russian patent no. 2178939 (27.01.2002, C1 Bull N3) 372

82. P. G. Zverev, T. T. Basiev, M. E. Doroshenko, V. V. Osiko: Barium tungstate Raman laser – A new coherent source for sodium star experiments, OSA Trends Opt. Photonics Ser. **34**, 348–354 (Opt. Soc. Am., Washington, DC 2000) 372, 378
83. T. T. Basiev, M. E. Doroshenko: Eye-safe mid IR $BaWO_4$ Raman laser oscillation in 1.5–2.15 μm spectral region, Optics of Lasers, Int. Conf., St. Petersburg, 2003 374
84. T. T. Basiev, T. T. Doroshenko, et al.: Short pulse Cr^{2+}:ZnSe laser oscillation under BaWO4 Raman laser pumping, J. Quant. Electron. (to be published)
85. P. G. Zverev, T. T. Basiev, A. A. Sobol, I. V. Ermakov, W. Gellerman: $BaWO_4$ crystal for quasi-CW yellow Raman laser, in Tech. Digest Adv. Solid-State Lasers (Opt. Soc. Am., Washington, DC 2001), pp. 124–125 374
86. P. Černý, H. Jelínková, T. T. Basiev, P. G. Zverev: Properties of transient and steady-state stimulated Raman scattering in $KGd(WO_4)_2$ and $BaWO_4$ tungstate crystals, in *Growth, Fabrication, Devices and Applications of Laser and Nonlinear Devices*, Proc. SPIE **4268**, 101–108 (2001) 376
87. P. Černý, H. Jelínková, J. Šulc, P. G. Zverev, T. T. Basiev: Evaluation of $BaWO_4$ steady-state Raman gain in single- and double-pass arrangement, in OSA Trends Opt. Photonics Adv. Solid-State Lasers **50**, (Opt. Soc. Am., Seattle, WA 2001) 376
88. P. Černý, P. G. Zverev, H. Jelínková, T. T. Basiev: Efficient Raman shifting of picosecond pulses using $BaWO_4$ crystal, Opt. Commun. **177**, 397–404 (2000) 376
89. P. Černý, P. G. Zverev, H. Jelínková, T. T. Basiev, L. I. Ivleva, V. V. Osiko: Comparison of stimulated Raman scattering of picosecond pulses in tungstate crystals, in *Nonlinear Materials, Devices, and Applications*, J. W. Pierce (Ed.), Proc. SPIE **3928**, 124–131 (2000) 376
90. P. Černý, H. Jelínková, P. Zverev, T. Basiev, V. Kubeček: Picosecond Raman gain of $CaCO_3$, $KGd(WO_4)_2$ and $BaWO_4$ crystals, in *Book of Abstracts*, paper CthE14, Conf. Lasers and Electro-Optics Europe, Nice, France; in CLEO Europe'2000 Tech. Digest (2000) p. 94 376
91. P. Černý, H. Jelínková, M. Miyagi, T. T. Basiev, P. G. Zverev: Efficient picosecond Raman lasers based on $BaWO_4$ and $KGd(WO_4)_2$ tungstate crystals emitting in 1.15 to 1.18-μm spectral region, accepted for presentation at LASE 2002, paper no. 4630-17 376, 378
92. P. Cherny, H. Jelinkova: Picosecond stimulated Raman scattering in $BaWO_4$ crystal with close to quantum limit efficiency, Tech. Digest, Int. Conf. Adv. Solid-State Lasers, Quebec, Canada, Feb. 2002 (Opt. Soc. Am., Washington, DC 2002) paper MB 11 376
93. A. A. Kaminskii, H. J. Eichler, K. Ueda, N. V. Klassen, B. S. Redkin, L. E. Li, J. Findeisen, D. Jaque, J. Garcia-Sole, J. Fernandez, R. Balda: Properties of Nd^{3+}-doped and undoped tetragonal $PbWO_4$, $NaY(WO_4)_2$, $CaWO_4$, and undoped monoclinic $ZnWO_4$ and $CdWO_4$ as laser-active and stimulated Raman scattering-active crystals. Appl. Opt. **38**, 4533–4546 (1999) 379, 380
94. J. Findeisen, H. J. Eichler, A. A. Kaminskii: Efficient picosecond $PbWO_4$ and two-wavelength $KGd(WO_4)_2$ Raman lasers in the IR and visible, IEEE J. Quant. Electron. **35**, 173–178 (1999) 379
95. A. A. Kaminskii, C. L. McCray, H. R. Lee, S. W. Lee, D. A. Temple, T. H. Chyba, W. D. Marsh, J. C. Barnes, A. N. Annanenkov, V. D. Legun, H. J. Eich-

ler, G. M. A. Gad, K. Ueda: High efficiency nanosecond Raman lasers based on tetragonal $PbWO_4$ crystals, Opt. Comm. **183**, 277–287 (2000) 379, 380
96. W. Chen, Y. Inagawa, T Omatsu, M. Tateda, N. Takeuchi, Y. Usiki: Self-stimulating, passively Q-switched, diode-pumped Nd^{3+}:$PbWO_4$ Raman laser, Techn. Digest, Int. Conf. Adv. Solid-State Lasers, Seattle, WA, Jan. 2001 (Opt. Soc. Am., Washington, DC 2001) 380
97. R. H. Stolen, E. P. Ippen, A. R. Tynes: Raman oscillation in glass optical waveguide, Appl. Phys. Lett. **20**, 62–65 (1972) 380
98. K. O. Hill, B. S. Kawasaki, D. C. Johnson: Low-threshold CW Raman laser, Appl. Phys. Lett. **29**, 181–183 (1976) 380
99. R. K. Jain, Ch. Lin, R. H. Stolen, W. Pleibel, P. Kaiser: A high-efficiency tunable CW Raman oscillator, Appl. Phys. Lett. **30**, 162–164 (1977) 380
100. D. C. Johnson, K. O. Hill, B. S. Kawasaki, D. Kato: Tunable Raman fiber-optic laser, Electron. Lett. **13**, 53–54 (1977) 380
101. R. K. Jain, Ch. Lin, R. H. Stolen, A. Ashkin: A tunable multiple Stokes CW fiber Raman oscillator, Appl. Phys. Lett. **31**, 89–90 (1977) 380, 381, 386
102. Ch. Lin, L. G. Cohen, R. H. Stolen, G. W. Tasker, W. G. French: Near- infrared sources in the 1–1.3 µm region by efficient stimulated Raman emission in glass fibers, Opt. Commun. **20**, 426–428 (1977) 380
103. Ch. Lin, R. H. Stolen, L. G. Cohen: A tunable 1.1-µm fiber Raman oscillator, Appl. Phys. Lett. **31**, 97–99 (1977) 380
104. H. Po, E. Snitzer, L. Tumminelli, F. Hakimi, N. M. Chu, T. Haw: Doubly clad high brightness Nd fiber laser pumped by GaAlAs phased array, Opt. Fiber Commun. Conf., Houston (1989) PD 7 381
105. H. Po, J. D. Cao, B. M. Laliberte, R. A. Minns, R. F. Robinson, B. H. Rockney, R. R. Tricca, Y. H. Zhang: High power neodymium-doped single transverse mode fiber laser, Electron. Lett. **29**, 1500–1501 (1993) 381
106. M. Muendel, B. Engstrom, D. Kea, B. Laliberte, R. Minns, R. Robinson, B. Rockney, Y. Zhang, R. Collins, P. Gavrilovich, A. Rowley: 35-Watts CW single-mode Ytterbium Fiber laser at 1.1 µm, CLEO'97, Tech. Digest (1997) paper CPD-30 381
107. D. Innis, D. J. DiGiovanni, T. A. Stasser, A. Hale, C. Headley, A. J. Stentz, R. Pedrazzani, D. Tipton, S. G. Kosinski, D. L. Brownlow, K. W. Quoi, K. S. Kranz, R. G.Huff, R.Espindola, J. D. LeGrange, G. Jacobovitz-Veselka: Ultrahigh-power single-mode fiber lasers from 1.065 to 1.472 µm using Yb-doped cladding-pumped and cascaded Raman lasers, CLEO'97, Tech. Digest (1997) paper CPD-31 381, 382
108. S. G. Grubb, T. Strasser, W. Y. Cheung, W. A. Reed, V. Mizrahi, T. Erdogan, P. J. Lemaire, A. M. Vengsarkar, D. J. DiGiovanni, D. W. Peckham, B. H. Rockney: High-power 1.48 µm cascaded Raman laser in germanosilicate fibers, Proc. Top. Meet. Opt. Amplifiers Appl. Davos (1995) paper SaA4, pp. 197–199 381, 382
109. Annual Report General Phys. Inst. Russ. Acad. Sci. 1993, sect. Optical fiber communication, integrated optics, p. 7 January 1994
E. M. Dianov, D. G. Fursa, A. A. Abramov, M. I. Belovolov, M. M. Bubnov, A. V. Shipulin, A. M. Prokhorov, G. G. Devyatykh, A. N. Gur'yanov, V. F. Khopin: Low-loss high germania-doped fiber: A promising gain medium for 1.3 µm Raman amplifier, Proc. 20th Europ. Conf. Opt. Commun., Firenze (1994) p. 427 381

110. S. Grubb, T. Erdogan, V. Mizrahi, T. Strasser, W. Y. Cheung, W. A. Reed, P. J.Lemaire, A. E. Miller, S. G. Kosinski, G. Nykolak, P. C. Becker: 1.3 μm cascaded Raman amplifier in germanosilicate fibers, Proc. Top. Meet. Opt. Amplifiers Appl., Breckenridge (1994) p. 187, paper PD 3-1 381, 382, 384
111. S. V. Chernikov, N. S. Platonov, D. V. Gapontsev, Do III Chang, M. J. Guy, J. R. Taylor: Raman fiber laser operating at 1.24 μm, Electron. Lett. **34**, 680–681 (1998) 382, 384
112. Do III Chang, Hak Kyu Lee, Kyong Hon Kirn: Cascaded Raman fiber laser operating at 1.48 nm, Electron. Lett. **35**, 1951–1952 (1999) 382
113. A. R. Chraplyvy, J. Stone: Synchronously pumped D_2 gas-in-glass fiber Raman laser operating at 1.56 μm, Opt. Lett. **9**, 241–242 (1984) 382
114. V. V. Grigoryants, B. L. Davydov, M. E. Zhabotinski, V. F. Zolin, G. A. lvanov, V. I.Smirnov, Yu. K. Chamorovski: Spectra of stimulated Raman scattering in silica fiber waveguides, Opt. Quantum Electron. **9**, 351–352 (1977) 382
115. J. Canning, R. Pasman, M. G. Seats: Photosensitisation of phosphosilicate fiber Bragg gratings, Topical Meeting: Photosesitivity and quadratic nonlinearity in glass waveguides, Fundamentals and applications, Portland (1995), Tech. Dig. Ser. **29**, 86–87 (1995) 383
116. E. M. Dianov, A. M. Prokhorov: Raman fiber laser (variants) and fiber Bragg grating, RU patent no. 2095902 (Nov. 10, 1997), US patent no. 5,838,700, (Nov. 17, 1998) 383
117. E. M. Dianov, M. V. Grekov, I. A. Bufetov, S. A. Vasiliev, O. I. Medvedkov, V. G. Plotnichenko, V. V. Koltashev, A. V. Belov, M. M. Bubnov, S. L. Semjonov, A. M. Prokhorov: CW high power 1.24 μm and 1.48 μm Raman lasers based on low loss phosphosilicate fiber, Electron. Lett. **33**, 1542–1543 (1997) 383
118. M. M. Bubnov, E. M. Dianov, O. N. Egorova, S. L. Semjonov, A. N. Guryanov, V. F. Khopin, E. M. DeLiso: Fabrication and investigation of single-mode highly phosphorus-doped fibers for Raman lasers, in *Advances in Fiber Optics*, Proc. SPIE **4083**, 12–22 (2000) 383
119. F. L. Galeener, J. C. Mikkelsen, R. H. Geils, W. J. Mosby: The relative Raman cross sections of vitreous SiO_2, GeO_2, B_2O_5 and P_2O_5, Appl. Phys. Lett. **32**, 34–36 (1978) 383
120. E. M. Dianov, I. A. Bufetov, M. M. Bubnov, A. V. Shubin, S. A. Vasiliev, O. I. Medvedkov, S. L. Semjonov, M. V. Grekov, V. M. Paramonov, A. N. Guryanov, V. F. Khopin, D. Varelas, A. Iocco, D. Costantini, H. G. Limberger, R.-P. Salathe: CW highly efficient 1.24 μm Raman laser based on low-loss phosphosilicate fiber, Tech. Digest Opt. Fibre Conf.'99 (1999) paper PD 25 383
121. E. M. Dianov, I. A. Bufetov, M. M. Bubnov, M. V. Grekov, A. V. Shubin, S. A. Vasiliev, O. I. Medvedkov, S. L. Semjonov, A. N. Gur'yanov, V. F. Khopin: Investigation of CW highly efficient 1.24 μm Raman laser based on low-loss phosphosilicate fiber, Proc. ECOC'99 **1**, 72–73 (1999) 383, 386
122. V. I. Karpov, E. M. Dianov, V. M. Paramonov, O. I. Medvedkov, M. M. Bubnov S. L. Semyonov, S. A. Vasiliev, V. N. Protopopov, O. N. Egorova: Laser-diode pumped phosphosilicate-fiber Raman laser with an output power of 1 W at 1.48 μm, Opt. Lett. **24**, 887–889 (1999) 384
123. E. M. Dianov, I. A. Bufetov, M. M. Bubnov, M. V. Grekov, S. A. Vasiliev, O. I. Medvedkov: Three-cascaded 1407 nm Raman laser based on phosphorus-doped silica fiber, Opt. Lett. **25**, 402–404 (2000) 386

124. A. S. Kurkov, E. M. Dianov, V. M. Paramonov, O. I. Medvedkov, A. N. Guryanov, A.Ẏu. Laptev, A. Umnikov, S. A. Vasiliev, N. N. Vechkanov, E. V. Pershina: 1.43 μm fiber laser for medical applications, in *Advances in Fiber Optics*, Proc. SPIE **4083**, 127–130 (2000) 386
125. E. M. Dianov, A. S. Kurkov, O. I. Medvedkov, V. M. Paramonov, O. N. Egorova, N. Kurukitkoson, S. K. Turitsyn: Raman fiber source for a range of 1.6–1.75 mm, Proc. Optical Fiber Conf. 2003, Atlanta, USA, March 25–27, 2003, paper MF26 387

Index